ELSEVIER

Chemical Geology 171 (2001) 147–171

CHEMICAL GEOLOGY
INCLUDING
ISOTOPE GEOSCIENCE

www.elsevier.com/locate/chemgeo

Alteration of monazite and zircon and lead migration as geochemical tracers of fluid paleocirculations around the Oklo–Okélobondo and Bangombé natural nuclear reaction zones (Franceville basin, Gabon)

Régis Mathieu [a,*], Lena Zetterström [b], Michel Cuney [a], François Gauthier-Lafaye [c], Hiroshi Hidaka [d]

[a] *CREGU-UMR G2R-7566, BP 239, Vandoeuvre-lès-Nancy Cedex F-54506, France*
[b] *Laboratory for Isotope Geology, Swedish Museum of Natural History, Stockholm S-10405, Sweden*
[c] *Centre de Géochimie de la Surface (CNRS-ULP), 1 rue Blessig, Strasbourg Cedex F-67084, France*
[d] *Department of Earth and Planetary Systems, Faculty of Science, Hiroshima University, Higashihiroshima J-739, Japan*

Received 12 July 1999; accepted 15 March 2000

Abstract

Large-scale light rare earth element (LREE), uranium, lead and phosphorus migration has been evidenced in the FA Lower Proterozoic sandstones of the Franceville basin (Gabon) hosting Oklo natural nuclear reaction zones (RZ) in relation with extensive accessory mineral alteration by highly saline diagenetic brines (28.7 wt.% NaCl eq. to 30 wt.% $CaCl_2$ eq.) at about 140°C and 1 kbar. Monazite is the most severely altered accessory mineral in the coarse-grained sandstones of the basal FA formation. Detrital monazite crystals are altered to Th–OH silicate microcrystalline phase with very low concentrations of U and LREE. The Th/La ratio increase from non-altered (Th/La ~ 0.27) to altered sandstones (Th/La ~ 1.14) shows that about 76% of the LREE was leached. This corresponds to the leaching of 2.01×10^9 metric tons at the scale of the FA formation in the Franceville basin. Similarly, the Th/U increase from monazite (Th/U = 18.6) to the Th-silicate phase (Th/U = 88.7) is interpreted as a result of an alteration by oxidizing brines with leaching of U together with LREE and P. It corresponds to the leaching of 9.06×10^6 metric tons of uranium. This amount of uranium largely exceeds the known uranium reserves from the Franceville basin.

In zircon crystals, the cores are generally homogeneous, weakly fractured and well preserved as attested by the Archean ages (2867 ± 24 and 2865 ± 51 Ma) obtained by ionic microprobe analysis on zircon of the FA Formation, respectively, from the marginal and central parts of the basin. Their composition corresponds to the pure end-member (Zr,Hf)(SiO_4), poor in Th and U (Th/U ~ 1). At the contrary, their rims, which present several growth zones with cracks fillings, are enriched in REE, P, Th and U with higher Th/U ratios (5–10).

Both altered monazite and altered zircon contain galena as numerous inclusions in the outer growth zones and as crack fillings. For example, in zircon, the Pb of galena crystals (3–23 wt.%) largely exceeds the amount of Pb (maximum 0.1

* Corresponding author. Fax: +33-3-83-91-38-01.
E-mail address: regis.mathieu@g2r.uhp-nancy.fr (R. Mathieu).

PII: S0009-2541(00)00245-X

wt.%) that would have been produced in situ by radioactive decay in this mineral. Nearly all the lead were introduced into altered zones of accessories. Dissolution of accessory minerals occurred at 2000 Ma, producing a porous and distorted crystal structure which has allowed a later incorporation of Pb. Galena inclusions in altered zircons located in the vicinity of reactor zones have radiogenic lead compositions. Altered zircon rims and galena inclusions in altered zircon located far from reactor zones have non-radiogenic Pb isotopic compositions, confirming the external origin of lead. Pb isotopic evolution models indicate a crystallization age sometime after 1000 Ma, both for galena located close to and far from U mineralizations and reactor zones, which may be synchronous with a regional extension event contemporaneous with intrusion of dolerite dyke swarms, between 1000 and 750 Ma, at the scale of the Franceville basin.

The present study also illustrates the different retention capacities of accessory mineral for elements representing analogs of the radiotoxic nuclides in the relatively extreme natural conditions created by the circulation of moderately hot and chloride-rich fluids during the diagenesis of a sedimentary basin.

Keywords: Monazite; Zircon; Alteration; Diagenesis; Migration; Lead; Oklo; Franceville

1. Introduction

Spontaneous natural fission reactions unique in the world occurred at 1.97 Ga (Ruffenach, 1979) in three U deposits of the Franceville basin, Gabon, namely Oklo, Okélobondo and Bangombé (Fig. 1). Natural fission reactions lasted for 10^5–10^6 years, producing a substantial amount of fission products (Naudet, 1991; Gauthier-Lafaye et al., 1996). Fifteen natural fission reactor zones (RZ) have been discovered since 1972 (Peycelon, 1995). Thirteen are known at Oklo, one at Okélobondo (RZ OK84bis) which represents, in fact, the South extension of the Oklo deposit, and one in the small uranium deposit of Bangombé located 20 km south of the Oklo–Okélobondo (Figs. 1 and 2). The usefulness of the Oklo deposit as a natural analogue for a geological repository of nuclear waste was recognized early (Walton and Cowan, 1975) and was extended at Okélobondo and Bangombé reactors zones in the 1980s (Gauthier-Lafaye et al., 1996). In this respect, the knowledge of the mineralogical settings of fission products is very important for a better understanding of the conditions of their migration or retention in a geological environment (Gauthier-Lafaye et al., 1996). Thus, all indications of radionuclide migration are of prime importance. U, Th and rare earth element (REE) are considered to be good chemical analogues of some radiotoxic nuclides (Krauskopf, 1986), and migration of these elements in the Franceville basin has therefore been particularly examined in the present study. Moreover, the importance of Pb mobilisations has been shown by the similarities between the behaviour of Pb and fissiogenic metals (Ru, Rh, Pd, Mo) during geochemical alteration of uranium ores. Although several studies at Oklo have demonstrated the transfer of fissiogenic products and their retention in some well defined mineral phases near RZ (apatite with fissiogenic Nd and Cs, Sère, 1996; La–Ce–Sr–Ca aluminous hydroxy phosphate with fissiogenic REEs and Zr, Dymkov et al., 1997; chlorite with Pu, Bros et al., 1993; or Pb release from uraninite, Janeczek and Ewing, 1995; Savary and Pagel, 1997), some problems about the migration of lead in the far-field of RZ remain debated. For example, Janeczek and Ewing (1995) state that reducing conditions prevent long distance migration of Pb. Raimbault et al. (1996) argue that an excess of lead in FA sandstones must be attributed to large-scale migration in the sedimen-

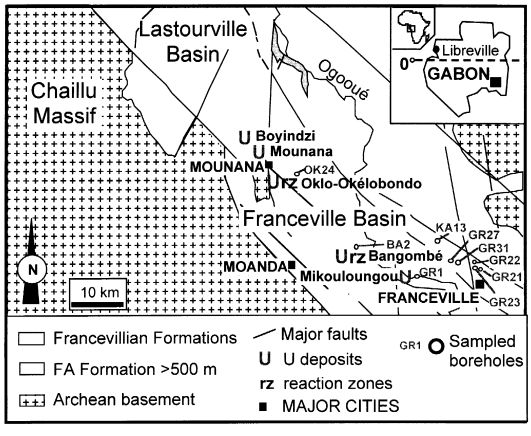

Fig. 1. Locations of uranium deposits and natural fission reactors (RZ) in the Franceville basin (Gabon) (modified from Weber, 1969).

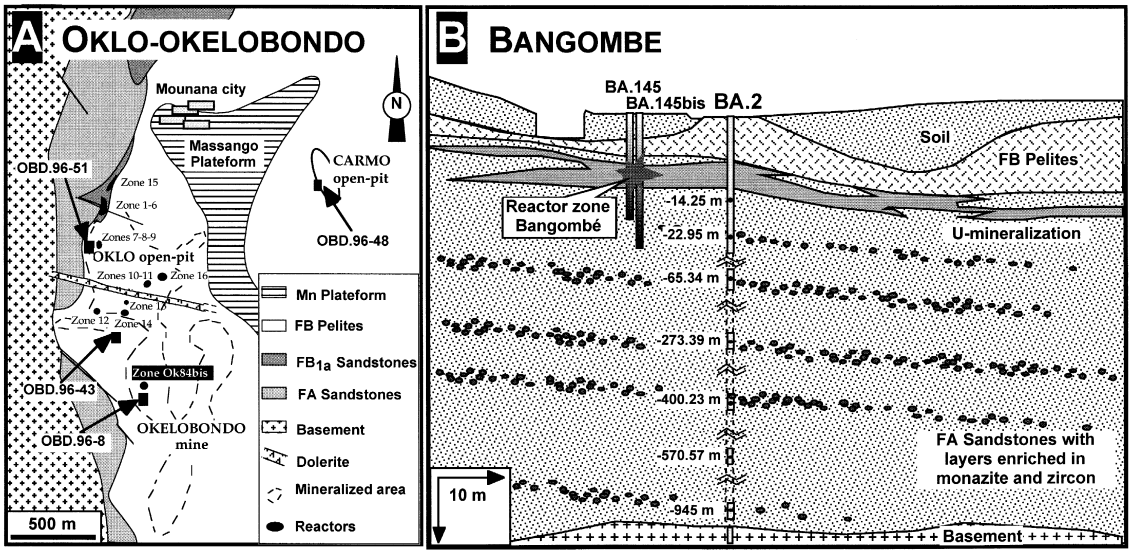

Fig. 2. Schematic location of samples containing zircons and monazites with galena inclusions: (A) OBD.96-8 in Okélobondo mine (near RZ OK84bis) and OBD.96-51 in Oklo open pit (near RZ 7-8-9) and (B) in BA.2 drill core (Bangombé): BA.2-14.25 m, BA.2-22.95 m, BA.2-65.34 m, BA.2-273.39 m, BA.2-400.23 m, BA.2-570.57 m, BA.2-945 m and BA.2-955 m.

tary basin. Savary and Pagel (1997) have demonstrated a Pb migration of around RZ16. However, most of the previous studies have been focused on the near field behaviour of the fissiogenic elements and their natural analogues.

The aim of this paper is to better assess the element migration at the scale of the Franceville basin with respect to those specifically related to the functioning of the natural nuclear reaction zones (RZ) from Oklo–Okélobondo and Bangombé U deposits. The present study discusses monazite and zircon alteration during diagenesis and the role of diagenetic fluid circulation on REE, U, Th, P, Zr geochemistry. U–Th–Pb chemical and U–Pb isotopes data are used to obtain the age of these accessory minerals and to discuss the timing of Pb migration in relation to this alteration event.

2. Geological setting

2.1. Deposition and diagenesis of the Francevillian series

The Francevillian sedimentary series unconformably overlies the Archean crystalline basement represented by the North Gabon massif to the north and the Chaillu massif to the south (Fig. 1). Several geochronological studies of the Archean basement in Gabon were performed by Caen-Vachette et al. (1988). The Chaillu massif, upon which the Francevillian sediments were deposited, yields Rb–Sr whole rock ages between 2.88 (gneiss) and 2.40 Ga (granitoid rejuvenated by tectonic movements). A Pb–Pb isochrone of Fe-rich amphibolites yielded the age of ca 2.7 Ga. This is the age of final metamorphism of the basement, since it coincides with biotite K–Ar ages of basement gneiss (Bonhomme et al., 1978). The Francevillian series is a 1000–4000 m thick, unmetamorphosed sequence of clastic and volcanoclastic sediments. The lithostratigraphic succession consists, from the bottom to top, of five major formations indexed FA to FE (Weber, 1969). The FA formation (100–1000 m thick), which lies unconformably upon the Archean metamorphic basement, is mainly composed of conglomerates and fine to coarse sandstones deposited in a fluvial to deltaic environment (Weber, 1969; Bonhomme et al., 1982). During the first diagenetic phase, quartz overgrowths are developed around detrital quartz grains and illite (mostly 1 Md illites) and chlorite are newly formed in the matrix (Gauthier-Lafaye and Weber, 1989). The burial depth reached about 4000 m and tempera-

tures 180–200°C (Openshaw et al., 1978; Gauthier-Lafaye and Weber, 1989). Sm/Nd isochrons of two authigenic clay fractions from the FB formation yielded ages of 2.099 ± 0.115 and 2.036 ± 0.079 Ga, which are considered to be the age of the early diagenesis (Bros et al., 1992). The FB formation is characterized by fine-grained marine sediments, mainly pelites and black shales, which are more or less calcareous at the base, changing to pure sandstones at the top of the formation. The FC formation is composed of massive dolomite and cherts interbedded with black shales, whereas the FD and FE formations are mainly composed of ignimbrites and epiclastic sandstones with interbedded shales.

2.2. The uranium deposits and natural fission reactions

The FA formation contains all the known uranium ore deposits of the Francevillian series, including the Oklo–Okélobondo and Bangombé deposits which host the natural fission reactors (Gauthier-Lafaye and Weber, 1989). The uranium concentration process has a complex history (Gauthier-Lafaye, 1986). Uranium is presumed to derive from the basal FA radioactive Th–U-rich conglomerates. Uranium deposition, located at the top of the FA formation, was dated by U–Pb discordia at 2.05 ± 0.03 Ga (Gancarz, 1978).

The high-grade uranium mineralization reached criticality at 1.97 ± 0.06 Ga (Ruffenach, 1979), shortly after or during the mineralizing event. Uraninite grains from reactor zone yielded similar ages, 1.968 ± 0.05 Ga and 2.018 ± 0.03 Ga (Holliger, 1988; Gauthier-Lafaye et al., 1996). If the uncertainties are taken into account, it is not possible to distinguish the different events.

2.3. The dolerite intrusion

Several episodes of Pb mobilization have been related to Late Proterozoic thermal events caused by regional extension in the Franceville basin. This extension was accompanied by the intrusion of numerous dolerite dykes, one of which crosscuts the Oklo deposit. These dykes have been dated by K–Ar (Bonhomme et al., 1978), Sm–Nd and U–Pb discordia (Bonhomme et al., 1982; Sère, 1996) to 1000–700 Ma. The difficulties in getting a precise age of these dykes could be due to prolonged heating in the basin. However, the dykes show signs of alteration which caused Ar loss. The lowest K–Ar ages around 500 Ma could indicate the age of this alteration event (Weber and Bonhomme, 1975). According to Holliger (1992), the thermal effect of the dolerite dyke intrusion on the uranium minerals of the deposits and the RZ was a major loss of lead.

3. Sample descriptions

Table 1 presents the location and a synthetic petrographic description of the samples, which have been selected according to their distance from the RZ to decipher the eventual influence of the nuclear reactions.

Near field samples (NRZ samples: 20 m maximum from RZ; Gerard et al., 1998) were taken in the vicinity of several reactor zones. Sample OBD.96-51 is a conglomerate from the Oklo open pit at 3 m from RZ 7, 8 and 9 (Fig. 2A). Sample BA.2-14.25 m from the Bangombé open pit is a silicified sandstones located at 8 m from RZ BA.145-10.5 m (Fig. 2B). Sample OBD.96-8 corresponds to a brecciated sandstone located near calcite veinlets between pelitic layers and mineralized sandstone layers, at 20 m from RZ OK84bis in the Okélobondo mine. Far field samples (FRZ samples) were taken in the FA silicified sandstones and microconglomerates enriched in monazite and zircon from the BA.2 drill core, selected at 20–945 m from the Bangombé RZ (Fig. 2B) and from GR drill cores located deeper in the center of the Franceville basin (Fig. 1). Two samples from Oklo open pit, OBD.96-43 and OBD.96-48,

Notes to Table 1:
NRZ: near the reactor zone; Gal: galena; RZ clay: “argile de pile”; FRZ: far from the reactor zone; RZ: reactor zone “facies pile”.
[a] Whole rock data.
[b] Electron microprobe data.
[c] Ion probe Pb–Pb data.
[d] SHRIMP U–Pb data.

Table 1
Samples description, location and mineralogic occurrences

U deposits	Stratigraphic position	Near/far reactor zone	Samples	Monazites alteration phases	Zircons alteration phases	Others
CARMO open pit	FB_2 sandstones	FRZ	OBD.96-48[a]	–	–	–
Oklo open pit	FB_1 sandstones	FRZ	OBD.96-43[a]	monazites[b]	–	–
	FA conglomerate	NRZ RZ 7-8-9	OBD.96-51	monazites[b] with Gal[c]	dark zircon core[b] with Gal[c]	–
				Th–U silicate alteration phase[b] with Gal[c]	Zr/(Th,U,REE)–Si/P phase[b] with Gal[c]	–
Okelobondo mine	mineralized FA sandstones	NRZ RZ OK84bis	OBD.96-8[a]	–	dark zircon core[b]	euhedral Gal[c] in calcite veinlets
				–	Zr/(Th,U,REE)–Si/P phase[b] with Gal[c]	euhedral Gal[c] in brecciated sandstones
Bangombe open pit	mineralized FA sandstones	NRZ RZ Bangombé	BA.2-14.25	–	–	native Pb[c] in interstitial position
	FA sandstones	FRZ	BA.2-22.95[a]	monazite[b]	–	–
				Th–U silicate alteration phase[b]	–	–
	FA sandstones	FRZ	BA.2-65.34[a]	monazite[b]	dark metamictized zircon growth zones[b,d] with Gal[c]	–
				Th–U–REE silicate alteration phase[b]	Zr/(Th,U,REE)–Si/P phase[b]	–
	FA sandstones	FRZ	BA.2-273.39[a]	monazite[b]	dark metamictized zircon growth zones[b] with Gal[c]	–
				Th–U silicate alteration phase[b]	Zr/(Th,U,REE)–Si/P phase[b]	–
	FA sandstones	FRZ	BA.2-278.2	monazite[b]	–	–
				Th–U silicate alteration phase[b]	–	
	FA sandstones	FRZ	BA.2-400.23[a]	monazite[b]	dark zircon core[b,d]	–
				Th–U silicate alteration phase[b]	–	–
	FA sandstones	FRZ	BA.2-570.57[a]	–	–	epigenetic Gal[c] in replacement of pyrite
	FA conglomerate	FRZ	BA.2-945	–	dark zircon core[b]	–
				–	Zr/(Th,U,REE)–Si/P phase[b] with Gal[c]	–
GR drill holes	FA sandstones	FRZ	GR.1-589.1[a]	Th–U silicate alteration phase[b]	dark zircon core[b,d]	–
	FA sandstones	FRZ	GR.1-716.4[a]	Th–U silicate alteration phase[b]	dark zircon core[b,d]	
	FA sandstones	FRZ	GR.21-510[a]	Th–U silicate alteration phase[b]	–	–
	FA sandstones	FRZ	GR.27-733.6[a]	Th–U silicate alteration phase[b]	–	Gal

were taken from FB_1 and FB_2 sandstones, respectively (Fig. 2A). Major and trace element abundances were determined in the sandstones and pelites.

Monazite and the associated monazite alteration phase occur as ~50–200 μm grains together with zircon as ~100–300 μm grains dispersed throughout the conglomerate matrix but may concentrate in heavy mineral bands of 300 μm in thickness. These accessory-rich layers extend laterally over some tens of meters, because they are found in several boreholes (BA near BA.2 borehole and GR near GR.31 borehole). U–Pb isotope analyses were performed on zircon cores. Monazite and zircon contain large amounts of galena crystals as veinlets and inclusions. Pb isotope analyses were performed on samples with galena or native lead in different relations to accessory minerals. Galena replacing pyrite (BA.2-570.57 m), galena inclusions in zircon (BA.2-65.34 m) and native Pb in interstitial position between detrital quartz grains (BA.2-14.25 m) just below the Bangombé RZ come from the FA sandstones in the BA.2 borehole. Galena inclusions and veinlets in monazite and zircon come from the conglomerate of the Oklo open pit (OBD.96-51). Galena crystals within zircon in the brecciated sandstone and galena crystal in a fibrous calcite veinlet come from mineralized FA sandstones in the near-field of OK84bis RZ (OBD.96-8).

4. Analytical procedures

Mineralogical and petrographical features of accessory minerals and associated alteration phases and their relationships with galena crystals were determined for 19 polished thin sections through optical observation in transmitted and reflected light and using a scanning electron microscope (SEM) with a backscattered electron (BSE) imaging, energy dispersive spectrometer (EDS) and X-ray mapping.

In situ quantitative elemental analyses were done with an automated Cameca SX50 electron micro-

Table 2
Instrumental parameters of Cameca SX50 electron microprobe for monazite and zircon analyses

Elts	Monazite			Zircon		
	Standards	C.T.	D.L.	Standards	C.T.	D.L.
Si	Orthose	60	40	Zircon	20	80
P	$KTiPO_4$	10	70	$RbTiPO_4$	20	80
Ca	Wollastonite	20	30	Wollastonite	10	50
Y	Garnet	60	130	Garnet	60	40
La	$LaRu_2Ge_2$	10	160	–	–	–
Ce	$CeRu_2Ge_2$	10	180	–	–	–
Pr	$PrRu_2Ge_2$	30	200	–	–	–
Nd	$NdRu_2Ge_2$	30	200	$NdRu_2Ge_2$	60	100
Sm	$SmRu_2Ge_2$	30	200	$SmRu_2Ge_2$	80	70
Gd	–	–	–	$GdRu_2Ge_2$	80	100
Al	–	–	–	Albite	20	50
Mg	–	–	–	Olivine	30	50
S	–	–	–	$SrSO_4$	10	430
Na	–	–	–	Albite	60	40
Rb	–	–	–	$RbTiPO_4$	60	50
Zr	–	–	–	Zircon	10	300
Hf	–	–	–	Zircon	30	100
Yb	–	–	–	$YbRu_2Ge_2$	80	80
Mn	–	–	–	$MnTiO_3$	20	300
Fe	–	–	–	Hematite	10	60
Pb	Galena	80	100	Galena	80	100
Th	Thorianite	80	100	Thorianite	80	90
U	Uraninite	80	100	Uraninite	80	100

Elts: analyzed elements; C.T.: counting times in seconds; D.L.: detection limits in parts per million.

probe (EMP) analyser (Joint Analytical Service, Nancy I University, France). An electron beam focused to approximately 6 μm^2 was used. Analytical conditions for monazite analysis were: 20 nA, 20 kV for major elements and 100 nA, 30 kV for trace elements. Analytical conditions for zircon analysis were: 10 nA, 20 kV for major elements and 100 nA, 30 kV for trace elements. Analyzed elements, standards used for the calibration of the microprobe, detection limits and counting times are reported in Table 2. Data were processed using the PAP program (Pouchou and Pichoir, 1984). To detect eventual contamination by galena, S was always measured and only analyses with no detected S (the detection limit was 0.043 wt.% of S) were used for this study.

The chemical composition of the FA sandstones and FB pelites and sandstones was determined using ICP-AES for major elements and ICP-MS for trace elements, following a procedure described by Govindaraju and Mevelle (1987).

To determine the origin of lead in galena inclusions and veinlets in accessories and in native lead, in situ Pb isotope analyses were conducted using a Cameca IMS1270 ion microprobe located at the Swedish Museum of Natural History, Stockholm (the NORDSIM facility). Thin sections were selected and prepared (cleaned and coated with ca. 25 nm of gold). For ca. 5-μm-large galena crystals and inclusions, as well as for the native Pb sample, a 4–5 μm (ca. 20 pA) large beam of primary O_2^- ions was used to sputter the secondary ions off the sample. A single electron multiplier was used in ion counting mode to measure the secondary ion beam intensities in the mass switching sequence: 204(Pb), 206(Pb), 207(Pb), 208(Pb). The counting rate of $^{206}Pb^+$ ions from galena, with a 20 pA primary beam, was ca. 5×10^5 cps. The mass resolution was set to 5600 and the uncertainties given on the measured ratios were 1σ standard errors. For the relatively low analytical precision in measured isotope ratios, there is a negligible mass fractionation associated with the sputtering process. Indeed, no systematic Pb isotope mass discrimination could be observed under the operating conditions adopted by Compston et al. (1984) and Belshaw et al. (1994). Mass discrimination less than 0.1% amu^{-1} has been reported for a Cameca ims1270 (Harrison et al., 1995). Even the larger mass discrimination of 0.2% amu^{-1}, reported by Cathelineau et al. (1990) for a Cameca IMS3*f*, is not resolvable for the data presented here. Thus, no correction for instrumental mass fractionation has been made for the measured Pb ratios.

5. Results

5.1. Monazite

Rounded, discrete grains of monazite in sandstones are generally accepted as detrital (Roscoe,

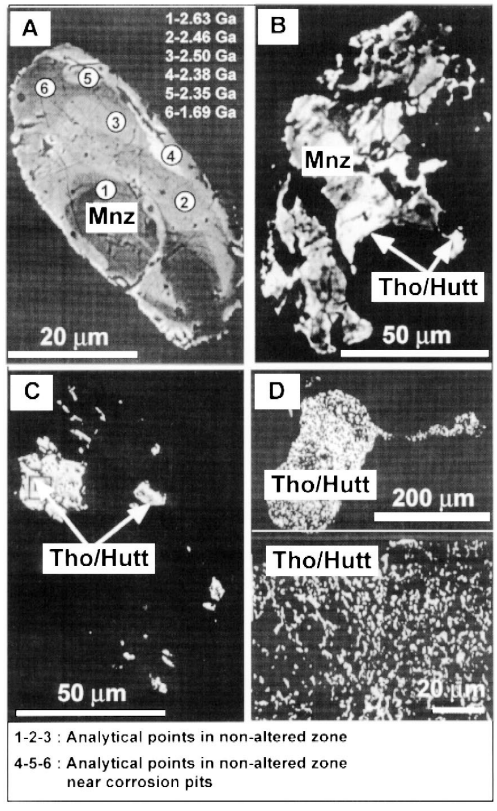

Fig. 3. BSE images of monazite and associated alteration phases: (A) unaltered monazite (Mnz) from the BA.2 drill core (−273.39 m) with rare corrosion pits; (B) highly corroded monazite crystals from the BA.2 drill core (−273.39 m); (C) strongly corroded monazite crystals mixed with a fine Th-silicate phase (Tho/Hutt) from BA.2 drill core (−22.95 m); and (D) Th-silicate xenomorphic phase with a composition close to thorite (or huttonite) (Th/Hutt) from BA.2 drill core (−65.34 m), with a very porous structure, located in intergranular spaces between the quartz grains of the sandstones.

1969). More than 90% of monazite crystals are dissolved to variably extend in the coarser-grained sandstones, but independently of the distance with the RZ. Moreover, the intensity of monazite alteration process increases in the center of the basin and with depth because of the higher abundance of Th-silicate alteration phase in GR samples. As shown in backscattered electron images (Fig. 3), the least modified grains contain isolated, partially euhedral grains identified by energy dispersive microprobe analysis as a Th-silicate phase (Tho/Hutt). Table 3 presents geochemical data obtained on monazite by electron microprobe.

Step 1 is represented by unaltered monazite with rare dissolution cavities (Fig. 3A). Unaltered detrital monazites present a predominant huttonitic substitution (up to 20%) and a very limited cheralitic substitution (Fig. 4). They have Th/U of about 18.6 and Th/La of about 0.33 (Table 4). Strongly corroded monazite crystals are intimately mixed with fine Th-silicate aggregates (Step 2) (Figs. 3B–C and 4). When monazite crystals are completely altered (Step 3), the residual Th-silicate phase, with very low concentrations of P and REE, may mimic the shape of the former crystals or may occur as independent xenomorphic porous aggregates in intergranular location between corroded detrital quartz grains (Fig. 3D). More than 90% of the Th-silicate phase corresponded to the huttonite component. The low totals of oxides obtained from microprobe analysis of the Th-silicate phase are due to its hydroxylation during metamictisation and its porous texture (Fig. 4). Th-

Table 3
Representative chemical analyses (wt.% oxides) for: (1) a detrital unaltered monazite (step 1); (2) a residual Th-silicate phase (step 3); (3) a zircon core; and (4) an altered zircon rim

	1	2	3	4
SiO_2	1.17	13.80	31.36	25.66
P_2O_5	27.45	4.85	0.226	1.437
CaO	0.718	2.749	0.273	0.777
Y_2O_3	0.787	2.077	1.077	1.234
La_2O_3	15.593	0.119	–	–
Ce_2O_3	29.620	3.500	–	–
Pr_2O_3	2.031	0.175	–	–
Nd_2O_3	10.302	0.637	0.156	0.327
Sm_2O_3	1.830	0.328	0.060	0.253
Gd_2O_3	–	–	0.149	0.418
Al_2O_3	–	−0.379	1.611	
MgO	–	–	0.012	0.024
SO_3	–	–	n.d.	0.379
Na_2O	–	–	n.d.	0.026
Rb_2O	–	–	0.098	0.101
ZrO_2	–	–	62.67	53.37
HfO_2	–	–	1.290	1.249
Yb_2O_3	–	–	0.126	0.125
MnO	–	–	0.064	0.333
FeO	–	–	0.402	0.664
PbO	0.806	0.112	n.d.	0.366
ThO_2	5.418	51.870	0.282	4.135
UO_2	0.253	0.552	0.123	0.220
Total oxides	97.43	82.41	98.35	91.17
Th/La	0.33	449.2	–	–
Th/U	21.35	93.68	2.29	18.74
LREE(PO_4)	93.4	11.1	–	–
(U + Th)(SiO_4)	5.0	80.3	–	–
$Ca_{0.5}(U + Th)_{0.5}(PO_4)$	1.6	8.6	–	–

n.d. — not detected.

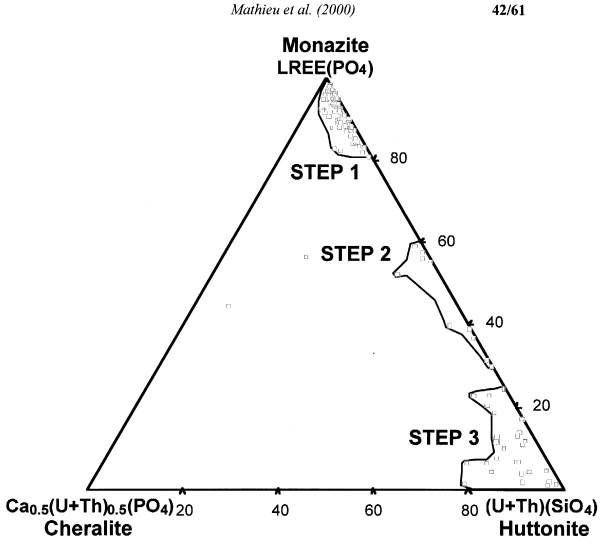

Fig. 4. Composition of monazite and alteration phases (three steps) in the monazite–cheralite–huttonite diagrams: (1) non-altered detrital monazite; (2) highly corroded monazite crystals mixed with a Th-silicate phase; and (3) Th-silicate residual phase after complete corrosion of monazite crystals.

silicate phases have Th/U ratios close to 88.7 and Th/La up to 44.9 (Table 4).

The occurrence of uranium-bearing organic matter together with Th-silicates in altered monazite crystals indicates that the alteration occurs prior to hydrocarbon migration and is probably contemporaneous with the early diagenesis (Fig. 5A). Principal multicomponent analysis performed on major and trace elements of altered monazite aggregates shows that leaching of P and light rare earth element (LREE) during monazite alteration is simultaneous with Si, U, Th, Pb, Ca and HREE relative enrichment. The lead increase is related to the formation of galena in dissolution cavities of monazite. HREE enrichment

Table 4
Th, La, LREE, U and P contents of the minerals (wt.%) and whole rocks (ppm) (n: number of analyses, ($\pm 1\sigma$) standard deviation

	Th	La	LREE	U	P	Th/La	Th/U
Monazite ($n = 94$)	4.04 ($\pm$0.62)	12.3 ($\pm$3.2)	48.8 ($\pm$4.3)	0.22 ($\pm$0.04)	11.8 ($\pm$1.48)	0.33 ($\pm$0.09)	18.6 ($\pm$3.8)
Th-silicate ($n = 27$)	43.1 ($\pm$5.9)	0.96 ($\pm$0.32)	5.14 ($\pm$1.45)	0.49 ($\pm$0.06)	2.31 ($\pm$0.92)	44.9 ($\pm$9.3)	88.7 ($\pm$25.2)
Unaltered Archean and Proterozoic metasediments[a] ($n = 104$)	10.4 ($\pm$4.1)	38.7 ($\pm$12.1)	–	2.7 ($\pm$0.75)	0.05 ($\pm$0.015)	0.27 ($\pm$0.04)	3.46 ($\pm$0.86)
Unaltered FB pelites[b] ($n = 2$)	11.25	44.9	178.5	2.6	0.03	0.27	4.49
Unaltered fine-grained FB and FA sandstones[b] ($n = 5$)	4.29 ($\pm$0.7)	16.8 ($\pm$3.9)	85.4 ($\pm$0.7)	1.67 ($\pm$0.25)	–	0.26 ($\pm$0.02)	3.03 ($\pm$0.92)
Altered coarse-grained FB and FA sandstones[b] ($n = 15$)	47.1 ($\pm$18.8)	36.2 ($\pm$14.1)	137 ($\pm$52)	3 ($\pm$1.2)	0.02 ($\pm$0.005)	1.14 ($\pm$0.15)	14.2 ($\pm$6.4)

[a] Data are taken from a compilation of Ribeiro (1999), Mc Lennan and Taylor (1979), Mc Lennan et al. (1995), Gibbs et al. (1986), Fayek and Kyser (1997), Fedo et al. (1996).

[b] Data from the present work (neutron activation; Raimbault, personal communication; and ICP-MS).

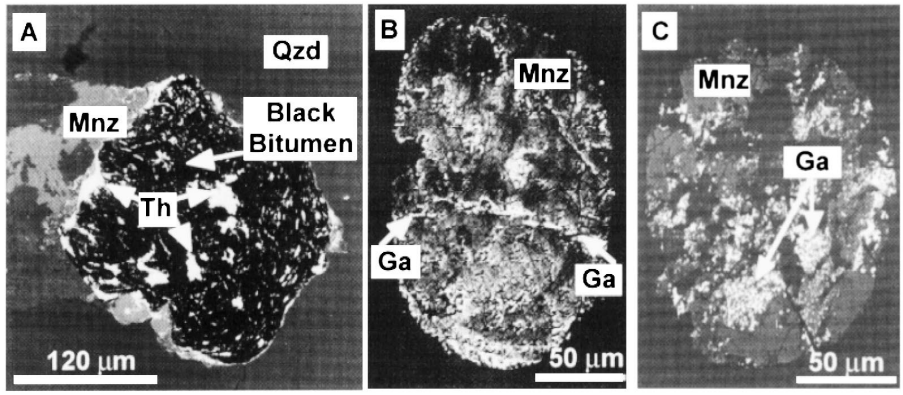

Fig. 5. BSE images showing: (A) organic matter (MO) surrounding Th-silicate phase (Th) issued from monazite (Mnz) alteration in FA sandstones (Qzd: detrital quartz) (BA.2-400.23 m sample); (B) galena (Ga) veinlets as white domains in monazite (Mnz) (OBD.96-51 sample); and (C) monazite (Mnz) with galena inclusions (Ga) (OBD.96-51 sample).

may correspond to a xenotime substitution in the Th-silicate phase. Ca enrichment appears to be better correlated with Pb and the Th-silicate phase. However, this enrichment may be secondary relative to the monazite alteration episode because the structure of the newly formed Th-silicate phase is very porous. Numerous altered monazite crystals contain galena inclusions either disseminated in the altered zones or occurring along cracks (Fig. 5B–C). This phenomenon is observed only relatively near a RZ (sample OBD96-51 from Oklo open pit).

The distribution of U–Th–Pb chemical ages of unaltered monazite (Step 1) calculated with the method of Montel et al. (1996) using U, Th and Pb contents and ^{235}U–^{238}U–^{232}Th radioactive decay constants is shown in Fig. 6. The statistical mode (the more repeated value obtained for pure monazite samples) is 2.51 ± 0.05 Ga. Ages of 2.7 up to 2.9 Ga are only preserved in few monazite crystals. A series of ages between 1.6 and 2.4 Ga corresponds to brighter zones of monazite located near dissolution cavities (points 4, 5 and 6; Fig. 3A).

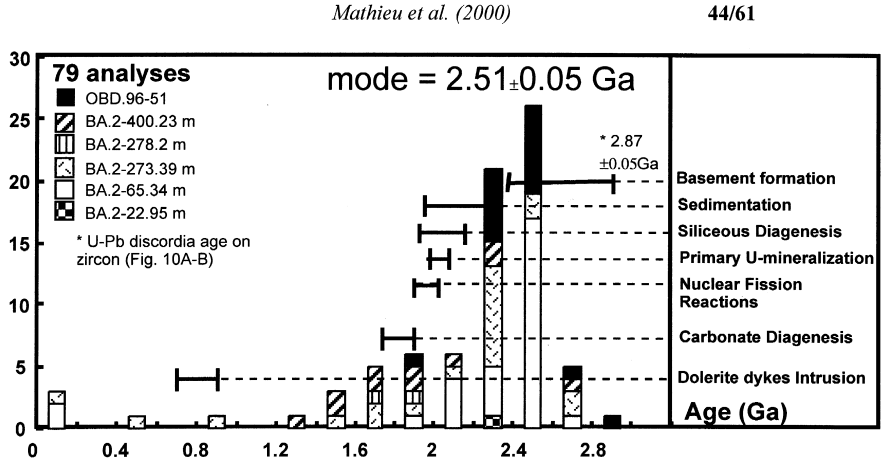

Fig. 6. Histogram of U–Th–Pb chemical ages of monazite (step 1) from the FA sandstones and conglomerates using the Montel et al. (1996) equation. Bars represent the ages of important geological events occurring in the area for comparison (compilation by Gauthier-Lafaye et al., 1996). These ages are lower than U–Pb discordia ages (2.87 Ga) obtained on zircon cores by SHRIMP measurements (see Fig. 10a–b).

5.2. Zircon

Zircon crystals display weakly fractured cores without galena inclusions and strongly fractured rims with several growth zones presenting large variations of average atomic number and numerous galena inclusions (Fig. 7). The proportion of galena in zircon ranges between 2 and 14 vol.% (Fig. 7). A 2D estimation of the galena area in a single zircon has been extrapolated at 3D by measurements on different sections. The chemical composition of the core corresponds to nearly pure zircon. The rims and the

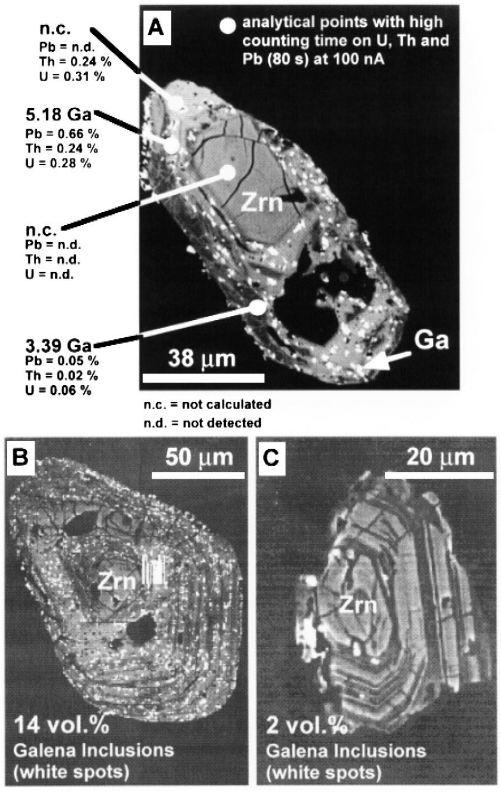

Fig. 7. BSE images of: (A) a zircon (Zrn) located in a conglomerate rich in accessory minerals, close to the unconformity with the basement (BA.2-945m sample). The core is dark, weakly fractured and devoid of galena inclusions (Ga). The rim, with several growth zones, is brighter nearly idiomorphic Zr/REE–Si/P phase containing galena inclusions. Galena inclusions correspond to the brightest spots. Pb–Th–U contents measured by electron microprobe give anomalous chemical ages (equation of Montel et al., 1996); (B and C) the two extreme cases of galena inclusions content (2–14 vol.%) in zircon crystals (Zrn), respectively, from OBD.96-51 and BA.2-945 m samples.

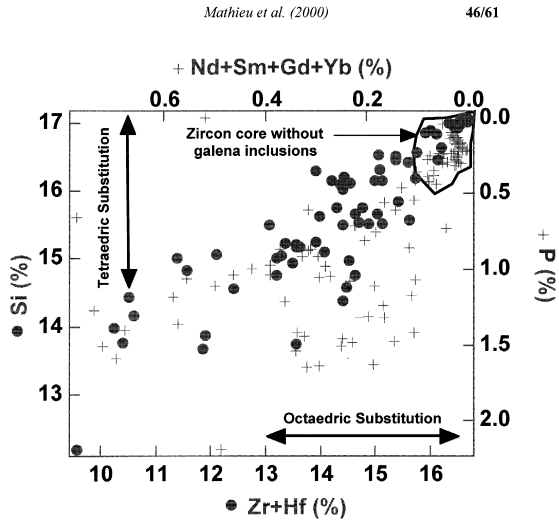

Fig. 8. Diagram showing: (1) the variation of Si vs. the sum of Zr and Hf (black circles) and (2) the variation of P vs. the sum of four major REE analyzed in zircon: Nd, Sm, Gd and Yb (grey crosses). A Si–P octahedral substitution and a Zr/Hf–REE tetrahedral substitution in the external growth zones of studied zircons are observed.

cracks are enriched in Nd, Sm, Gd, P, U, Th and Pb (Table 3). The chemical composition of this zone is interpreted as resulting from an alteration episode with P ⇔ Si tetrahedral substitution and Nd, Sm, Gd, Yb ⇔ Zr, Hf octaedric substitution (Fig. 8).

The decrease of Zr + Hf in the alteration rims also corresponds to a decrease in the total of oxides, probably caused by metamictisation related to higher U and Th contents and hydroxyl groups incorporation.

Zircon cores are generally poor in Th and U (Th/U ~ 2.3) that generally are below the analytical detection limit of 90 ppm (Table 2), whereas zircon rims are enriched in Th and U with higher Th/U ratios (18.7) (Table 3). No differences appear between zircons from near RZ or far from them.

5.3. Whole rock data

In order to evaluate quantitatively element loss from the host sandstones during monazite alteration, whole rock analyses have been performed and compared to the data on the Francevillian series at Okélobondo obtained by Raimbault (1998) and nu-

merous Archean and Proterozoic metasediments in the world (Table 4). FA and FB fine-grained sandstones, in which monazite is not altered, and FB pelites of the Franceville basin have similar whole rock Th/La ratios (0.26–0.27) as the Archean and Proterozoic quartzites and shales all over the world (Table 4; Fig. 9). FA and FB coarse-grained sandstones present Th/La ratios ranging from 0.97 to 1.48 according to the degree of monazite alteration (around 1.14 in average) (Table 4; Fig. 9). Higher Th/La of altered sandstones cannot be explained by a difference in the nature of the Th and LREE host minerals prior to alteration — mostly monazite in coarse-grained sandstones and mostly adsorbed on clay minerals in finer-grained sandstones and pelites — because: (i) Archean and Proterozoic quartzites and shales present the same low average Th/La ratios all over the world and (ii) the few unaltered coarse-grained sandstones rich in monazite show also similar low Th/La ratios. This alteration has leached

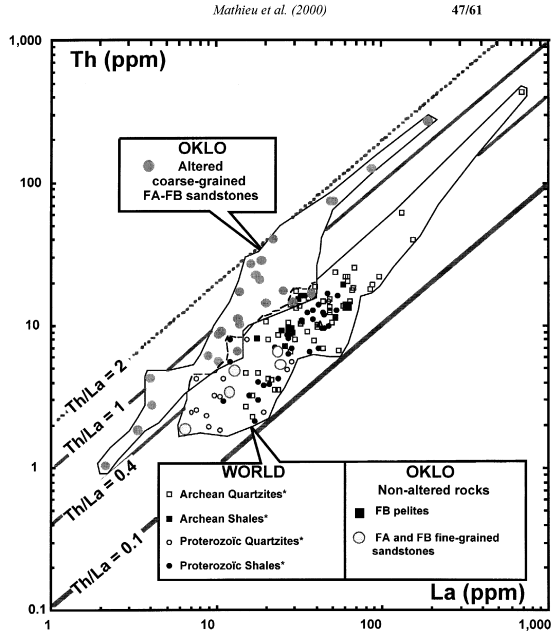

Fig. 9. Comparison of the Th/La ratios between coarse-grained silicified sandstones of the FA and FB formations, shales and fine-grained sandstones from the Franceville basin (present study) and quartzites and shales from several Archean and Proterozoic sedimentary basin. * Data are taken from a compilation of Ribeiro (1999), Mc Lennan and Taylor (1979), Mc Lennan et al. (1995), Gibbs et al. (1986), Fayek and Kyser (1997) and Fedo et al. (1996).

La, hence LREE, essentially from detrital monazite crystals from FA and FB coarse-grained sandstones.

5.4. U–Pb and Pb–Pb isotope data

SHRIMP U–Pb dating of cores of detrital zircon crystals was conducted to put time constraints on the age of zircon crystallization in the basement. U–Pb zircon data from deep BA.2 (65.34 and 400.23 m) and GR.1 (589.1 and 716.4 m) FRZ borehole samples are reported in Table 5. These data are used to plot two discordias with upper intercepts ranging from 2865 ± 51 to 2867 ± 24 Ma, respectively, for BA.2 and GR.1 samples, at 95% confidence (Fig. 10). Thus, zircon cores crystallized around 2.87 ± 0.05 Ga.

SIMS Pb isotope analyses of galena inclusions and veinlets in zircon and monazite, zircon, monazite, sulfides and native lead were conducted to put isotopic constraints on the origin of Pb and the timing of galena crystallization in relation to the monazite and zircon alteration (Fig. 11). Pb isotope data from NRZ samples (BA.2-14.25 m near BA.2 RZ-Bangombé, OBD.96-8 near OK84bis RZ-Okélobondo and OBD.96-51 near RZ 7-8-9-Oklo) are given in Tables 6 and 7. Pb data from galena are plotted in a $^{207}Pb/^{206}Pb$ vs. $^{204}Pb/^{206}Pb$ diagram in which data form two well defined groups (Fig. 12).

Near the uranium deposits, the 5-μm-large crystal of native lead, occurring inside As–Ni–Co–Fe sulfides from the NRZ BA.2-14.25 m sample, has a very radiogenic Pb ($^{204}Pb/^{206}Pb = 0.00062$). Enclosing sulfides present a slightly higher $^{207}Pb/^{206}Pb$ than the native lead. Galena inclusions in zircon NRZ OBD.96-8 have also a highly radiogenic lead isotopic composition ($^{204}Pb/^{206}Pb$ down to 0.00014), and low $^{207}Pb/^{206}Pb$ (ca 0.13), whereas galena inclusions in samples NRZ OBD.96-51 have a less radiogenic lead ($^{204}Pb/^{206}Pb$ min = 0.00076), as well as a higher $^{207}Pb/^{206}Pb$ (ca 0.17). Similar values were also obtained for the zircon and monazite matrix surrounding galena inclusions. It should be noted that 2σ errors on analyses in altered zircon and monazite are higher than for galena inclusions, and that the $^{204}Pb/^{206}Pb$ on average is ca. 10% lower.

Far from the uranium deposits, galena inclusions and veinlets from the FRZ borehole samples (BA.2-

Table 5
U contents and U–Pb isotopic ratios of zircon cores (SHRIMP analysis)

Number	Depth (m)	U (ppm)	$\pm 1\sigma$	$^{207}Pb/^{235}U$	$\pm 1\sigma$	$^{206}Pb/^{238}U$	$\pm 1\sigma$	Age 206/238	$\pm 1\sigma$
GR.1-1	589.1	118.3	5.62	15.569	0.464	0.555	0.022	2846	101
GR.1-2	589.1	116.2	3.35	15.403	0.638	0.557	0.030	2856	137
GR.1-3	716.4	66.4	4.54	16.121	0.424	0.552	0.027	2834	126
GR.1-4	716.4	386.0	34.19	11.579	0.797	0.440	0.042	2351	234
GR.1-5	716.4	442.4	42.01	8.561	0.724	0.329	0.037	1833	235
GR.1-6	716.4	89.4	2.09	12.766	0.674	0.458	0.029	2430	146
GR.1-7	716.4	117.3	3.37	8.303	0.073	0.290	0.014	1639	77
GR.1-8	716.4	206.7	11.41	9.291	0.718	0.336	0.028	1868	160
GR.1-9	716.4	242.3	10.06	10.568	0.873	0.375	0.035	2054	205
GR.1-10	716.4	129.2	2.41	16.637	0.521	0.581	0.026	2951	117
GR.1-11	716.4	191.8	13.97	13.558	0.925	0.475	0.052	2507	293
BA.2-1	400.23	217.4	9.95	11.476	0.739	0.389	0.030	2118	163
BA.2-2	400.23	2283.9	170.11	1.067	0.114	0.058	0.009	363	75
BA.2-3	400.23	6644.1	462.03	0.100	0.005	0.010	0.002	62	14
BA.2-4	400.23	378.8	8.06	11.535	0.443	0.424	0.020	2279	102
BA.2-5	400.23	197.3	10.35	11.755	0.656	0.418	0.027	2252	144
BA.2-6	400.23	941.4	39.12	1.002	0.067	0.051	0.006	318	48
BA.2-7	400.23	7044.1	502.20	0.097	0.012	0.010	0.002	64	17
BA.2-8	400.23	112.3	8.94	8.999	0.900	0.325	0.039	1816	247
BA.2-9	65.34	481.6	19.46	10.440	0.414	0.380	0.025	2076	133
BA.2-10	65.34	179.1	7.36	12.795	0.804	0.444	0.039	2366	210
BA.2-11	65.34	559.7	33.81	8.691	0.232	0.335	0.027	1865	156

65.34 m and BA.2-570.57 m) have non-radiogenic Pb isotopic compositions, similar to common Pb of average crust. They have $^{204}Pb/^{206}Pb$ between 0.047 and 0.055. This composition is found in both galena inclusions and the surrounding altered zircon. Since zircon normally has very radiogenic Pb compositions, this indicates that the major part of the Pb is not produced in situ, and therefore has an external origin. Epigenetic galena in a conglomerate at 570 m have Pb with somewhat higher radiogenic ($^{206}Pb/^{204}Pb \sim 21$) and lower $^{207}Pb/^{206}Pb$ (ca. 0.76). The 2σ errors on $^{204}Pb/^{206}Pb$ are around 1%, but for "pyrite–galena intergrowth", the error is almost 3%. These errors cause the error envelope around a plotted "isochron" to cover almost all of the Stacey and Kramers (1975) growth curve, as well as very large errors on calculated model ages. Thus, FRZ Pb data cannot give any clear age determinations, but possible interpretations are discussed in Section 6.4.

The Pb–Pb results show clearly that galena NRZ and FRZ have different sources. The very radiogenic composition NRZ implies that Pb came either from the uranium deposit in the surrounding rocks, or from monazite and zircon. Common Pb FRZ, on the other hand, implies that the source is not the uranium ore, but rather a source more similar to average crust.

6. Discussion

Although LREEs are generally considered immobile, several studies have shown that LREE may be mobile during hydrothermal alteration of igneous rocks under specific conditions (Mc Lennan and Taylor, 1979; Alderthon et al., 1980; Jefferies, 1985; Wood and William-Jones, 1994). In clastic sediments, according to Smith and Barreiro (1990), Naudet (1991), Akers et al. (1993) and Kingsbury et al. (1993), monazite, which represents by far the main LREE-bearing phase, would be altered during diagenesis and very low-grade metamorphism. But the alteration reaction has never been clearly observed in these studies. However, detrital monazite

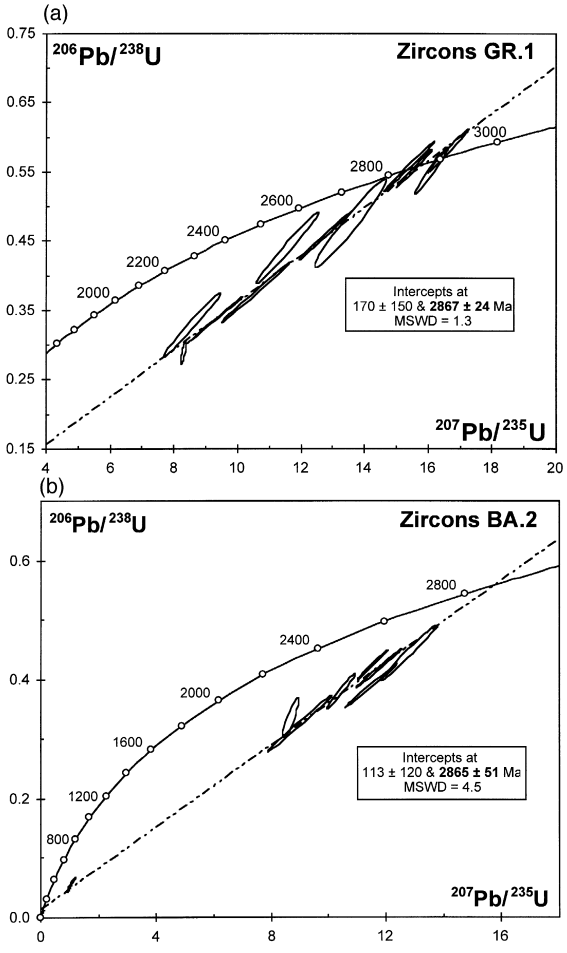

Fig. 10. Plots of $^{206}Pb/^{238}U$ vs. $^{207}Pb/^{235}U$ of zircon cores from: (a) deep GR.1 (589.1 and 716.4 m) FRZ samples and (b) BA.2 (65.34 and 400.23 m) FRZ samples. Data point error ellipses are 1σ.

dissolution and partial replacement by (U,Th)(SiO_4) have been described in conglomerates from the Quirke U-ore zone of Elliot Lake (Canada) (Robinson and Spooner, 1984) or from the Witwatersrand Au–U system (South Africa) (Schidlowski, 1981; Dimroth, 1979). But, these studies gave no evaluation of an eventual REE leaching from the whole sedimentary rock system during monazite alteration.

On the Oklo example, we will now quantify the magnitude of LREE and U migration and determine the nature of the fluids involved in this process at the scale of heavy mineral alteration (micrometer scale) and at the scale of the whole rock alteration (kilometer scale).

6.1. Accessory minerals alteration, element mobility and trapping phases

Our study clearly shows that monazite and zircon alteration did occur at the scale of the Franceville basin mainly in the coarser-grained FA sandstones.

Fluid circulation in the vicinity of radioactive minerals (especially zircon) is enhanced due to microfissures caused both by radiation damage in the surrounding rock and volume increase following hydration of the metamict mineral. These microfissures may represent preferential channels for circulating fluids. Our study has also evidenced that monazite alteration is characterized by the leaching of P and U together with LREE. Th and a small amount of LREE remain essentially in situ both are recombined with Si brought by the alteration fluid together with a small amount of HREE. During monazite alteration, Th is considered as an immobile element. However, a very thin layer of a Th-silicate phase (Fig. 13C–D) deposited at the surface of a single zircon crystal from FA sandstones may indicate a very limited mobility of thorium during the alteration process. Pb and Ca enrichments are also observed, but are not necessarily contemporaneous with this alteration.

Altered zircons are also found both near and far from any RZ. Bright zones corresponding to zircon rims contain more Th and U and probably are metamict. Ca, P, Nd, Sm, Gd, Yb, Fe, Ti and Y have been incorporated into the rims. No chemical difference is observed between these rims and veinlet infillings. Zircon leaching has only allowed the release of low quantities of Si and Zr in brines (respectively, 6 wt.% SiO_2 and 10 wt.% ZrO_2 deduced from the difference of average contents in zircon core and zircon rim; Table 3). Galena inclusions and veinlets are mainly observed in the altered rims of the zircon crystals in the FA sandstones. A zircon crystal with an average U content of about 1000 ppm and 2500 ppm of Th will have after 2.87 Ga less than 1000 ppm Pb. As the proportion of galena in zircon may exceed 2 vol.% up to 14 vol.% (Fig. 7), we come to the important conclusion that the lead has to derive from external sources. From the num-

bers above, Pb produced in situ is at maximum ca. 3% (maximum 0.1 wt.%) of the total amount of Pb. Other arguments favor an external origin for Pb of galena: (i) small galena crystals may occur between detrital quartz grains in brecciated sandstones, near zircon Zrn3 (Fig. 11D) and (ii) euhedral galena crystals were observed in fibrous calcite veinlets (Fig. 11F).

The phosphate released from monazite dissolution has been trapped in several secondary phosphate minerals (florencite, apatite, hydroxyapatite, zirconophosphate, etc.) in all FA sandstones, both near and far from reactor zones. The interstitial phase of the FA sandstones contains idiomorphic fluorapatite crystals. Part of the P and LREE leached from monazite are trapped locally in florencite microcrystals surrounded by authigenic chlorite in mineralized FA sandstones (Fig. 13B). Several evidences of (U,Zr)-silicate phase trapped in chlorite fibers (Fig. 13A) of the chlorite–quartz veins, overall the FA sandstones, are another arguments in favor of Zr mobility during vein infilling by diagenetic fluids. Similarly, Raimbault et al. (1996) have found a secondary xenomorphic Zr/(Y,Sc,U,Ca,LREE)-Si/P phase in FA sandstones. Janeczek and Ewing (1996b) have described Zr–Si–LREE-rich fluorapatite with hematite inclusions. Below the Bangombé RZ, Janeczek and Ewing (1996a) have described P–S–LREE-rich coffinite.

All petrographic relations: (1) alteration of accessories occurring before organic matter migration; (2) quartz filling; and (3) secondary phases (hydroxyfluoapatite, zirconosilicate, zirconophosphate, Th-silicate) crystallization confirm that early diagenesis was the main process responsible for LREE, P, Zr and U leaching overall the Franceville basin before the mineralization and criticality. Galena could be crystallized, with external Pb, in altered zones of accessory minerals simultaneously or later than the alteration.

6.2. Nature of fluids responsible for the leaching of U, LREE, P, Zr and Si

As no LREE- and P-bearing mineral was newly formed in the vicinity of dissolved monazite crystals, LREE and P seem to have been extensively leached out by diagenetic fluids. The diagenetic fluids correspond to highly saline (from 28.7 wt.% NaCl eq. to 30 wt.% $CaCl_2$ eq., rich in Li–Br–SO_4) brines (135–155°C) at 1000 bar (Mathieu et al., 2000). During the early diagenesis, these highly saline diagenetic brines have partly to completely altered accessory detrital minerals. Because they are responsible for the Th/U increase, these fluids must have been oxidizing in order to leach U together with P and LREE from monazite. Similar temperature conditions were given by Gauthier-Lafaye and Weber (1989) who have shown that NaCl-dominated brines from the Franceville basin have interacted with sandstones and clays at maximum temperatures around 140–150°C. Consequently, uranyl chloride complexes may be important in the leaching of uranium. Zircon solubility is increased in F-rich basinal brines (Rubin et al., 1993). In the Franceville basin, F may originate from chloritization of biotites from the Archean basement and/or from the sandstones detrital phases during early diagenesis.

The fluids deriving from accessories alteration contain uranyl phosphate complexes because monazite alteration released P together with LREE and U into solution. Moreover, the crystallization of fluorapatite in vuggy quartz–iron hydroxide veins and florencite in FA sandstones indicates the presence of P and F in basinal brines.

The alteration stopped when low saline fluids, heated to 190–210°C in the basement (Mathieu et al., 2000), were injected into the basin. These fluids caused intense silification which reduced the porosity significantly and hindered further fluid circulation.

6.3. Magnitude of the LREE and U migration

A quantitative estimation of the leaching of LREE and U from the FA formation presenting monazite alteration can be obtained by taking Archean and Proterozoic metasediments from the literature as a reference and Th as an immobile element. La was chosen to be representative of the LREE content of the rock assumed to be completely held in monazite. This hypothesis is supported by the fact that the average Th/La ratio of non-altered monazite (Th/La ~ 0.33; Table 4) in the FA sandstones is close to that of the FA and FB fine-grained sandstones and FB pelites of the Franceville basin area

and to the average Th/La ratios of the Archean and Proterozoic quartzites and shales from the literature (Mc Lennan and Taylor, 1979; Mc Lennan et al., 1995; Gibbs et al., 1986; Fedo et al., 1996; Fayek and Kyser, 1997; Ribeiro, 1999). FA and FB fine-grained sandstones, in which monazite is not altered, and FB pelites of the Franceville basin have similar whole rock Th/La ratios (0.26–0.27) as the Archean and Proterozoïc quartzites and shales all over the world (Table 4; Fig. 9). FA and FB coarse-grained sandstones and conglomerates present Th/La ratios ranging from 0.97 to 1.48 according to the degree of monazite alteration (1.14 in average) (Table 4; Fig. 9). Higher Th/La of altered sandstones cannot be explained by a difference in the nature of the Th and LREE host minerals prior to alteration — mostly

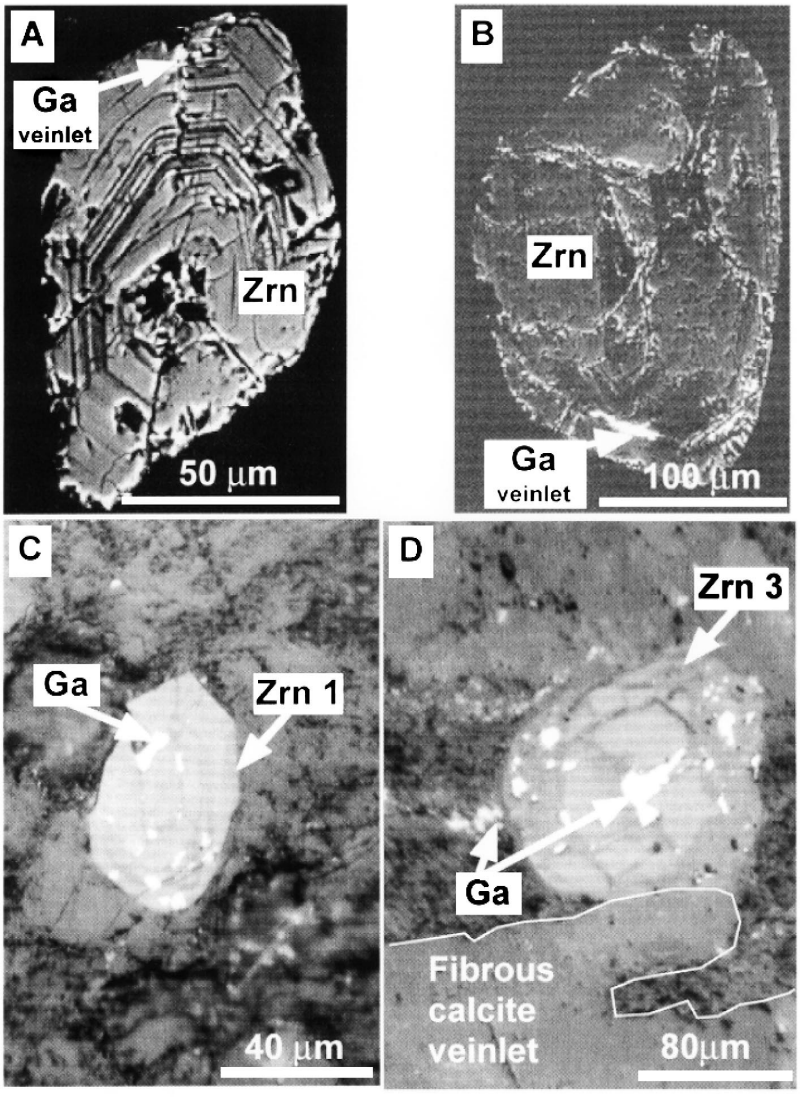

Fig. 11. BSE images and reflected light photomicrographs showing the location of: (A and B) galena veinlets (Ga) analyzed with ion microprobe (OBD.96-51 sample); (C, D and F) galena inclusions (Ga) analyzed with ion microprobe in zircon crystals (Zrn1 and Zrn3) and fibrous calcite veinlet (OBD.96-8 sample); (E) galena inclusions (Ga) analyzed with ion microprobe in zircon crystals (Zrn) (BA.2-65.34 m sample); (G) native lead surrounding by polymetallic sulfurs (BA.2-14.25 m sample) analyzed with ion microprobe; and (H) epigenetic galena (Ga) in pyrite crystals (Py) analyzed with ion microprobe (BA.2-570.57 m sample).

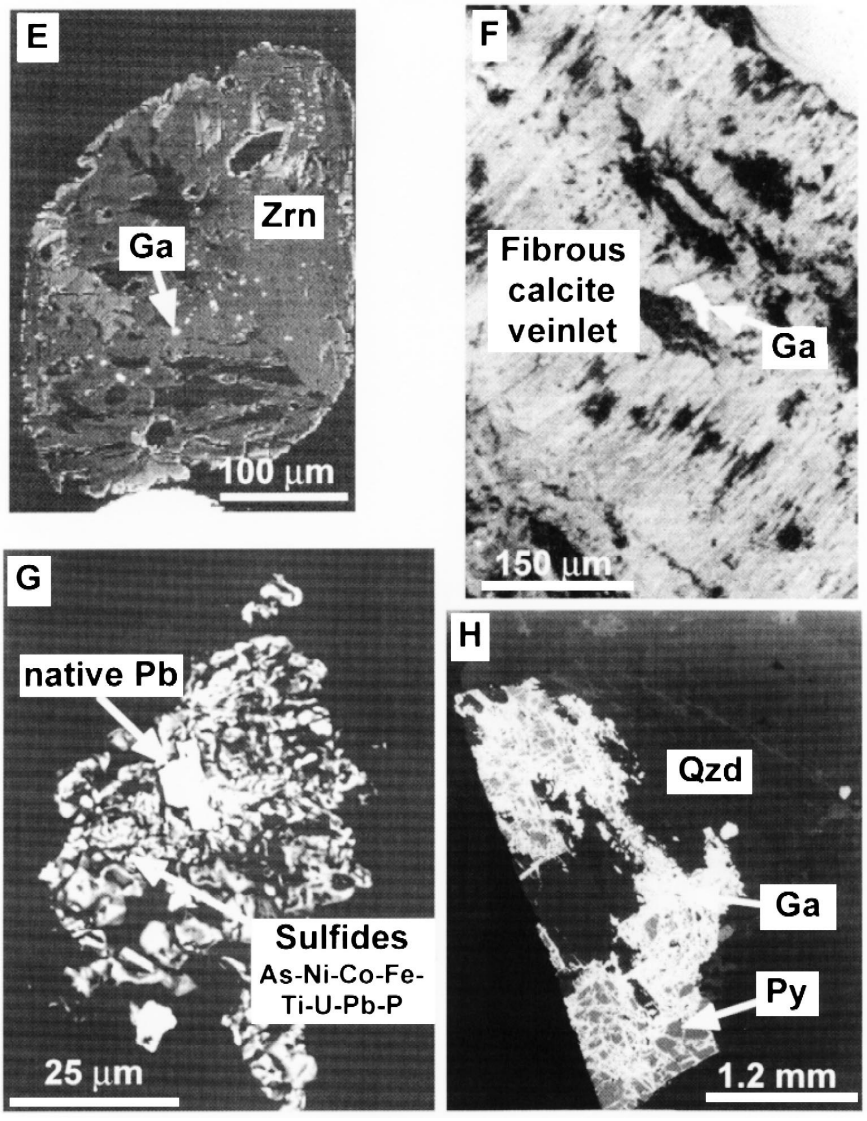

Fig. 11 (*continued*).

monazite in coarse-grained sandstones and mostly adsorbed on clay minerals in finer-grained sandstones and pelites — because: (i) Archean and Proterozoic quartzites and shales present the same low average Th/La ratios all over the world and (ii) the few unaltered coarse-grained sandstones rich in monazite also show similarly low Th/La ratios. Taking a Th/La ratio of 0.27 as the initial ratio of altered sandstones, the magnitude of the LREE depletion in the FA sandstones can be calculated.

A balanced volume of coarse-grained FA and FB sandstones concerned by the LREE leaching in the Franceville basin before U mineralization has been estimated at about 1850 km^3 considering two zones: (i) a border zone (2000 km^2 and 750 m thick) with 80 vol.% of coarse-grained sandstones and (ii) a central zone (1000 km^2 and 1 km thick) with 65 vol.% of coarse-grained sandstones. Assuming a density of 2.5 (Daly et al., 1966), the FA sandstones represent a mass of 4625.10^9 tons.

Table 6
Pb isotopic ratios of galena, native lead, sulfides, zircon and monazite (SIMS analysis)

Number	Location	Distance/RZ	Sample	Rock type	Mineral	$^{207}Pb/^{206}Pb$	$\pm 2\sigma$	$^{208}Pb/^{206}Pb$	$\pm 2\sigma$	$^{204}Pb/^{206}Pb$	$\pm 2\sigma$
1	OK84bis	NRZ	OBD.96-8	Sandstone + pelite	Galena 1	0.137	0.002	0.0096	0.0004	0.00020	0.00003
2	OK84bis	NRZ	OBD.96-8	Sandstone + pelite	Galena in Zircon1	0.130	0.003	0.0089	0.0002	0.00016	0.00002
3	OK84bis	NRZ	OBD.96-8	Sandstone + pelite	Galena in Zircon 3	0.132	0.002	0.0088	0.0002	0.00014	0.00001
4	Bangombe	NRZ	BA.2-14.25 m	Silicified sandstone	Native lead in As–Ni–Co–Fe sulfides	0.147	0.001	0.0329	0.0003	0.00062	0.00004
5	Bangombe	NRZ	BA.2-14.25 m	Silicified sandstone	As–Ni–Co–Fe sulfides	0.152	0.004	0.0292	0.0011	0.00092	0.00010
6	Oklo open pit	NRZ	OBD.96-51	Conglomerate	Galena in crack in zircon	0.169	0.001	0.0573	0.0003	0.00076	0.00002
7	Oklo open pit	NRZ	OBD.96-51	Conglomerate	Zircon surrounding galena	0.170	0.004	0.0603	0.0010	0.00069	0.00021
8	Oklo open pit	NRZ	OBD.96-51	Conglomerate	Galena in crack in monazite	0.167	0.001	0.3116	0.0028	0.00080	0.00005
9	Oklo open pit	NRZ	OBD.96-51	Conglomerate	Monazite surrounding galena	0.167	0.004	1.1850	0.0148	0.00062	0.00010
10	Oklo open pit	NRZ	OBD.96-51	Conglomerate	Galena in monazite	0.163	0.001	0.0661	0.0007	0.00083	0.00003
11	Oklo open pit	NRZ	OBD.96-51	Conglomerate	Monazite with galena	0.170	0.002	0.2157	0.0013	0.00085	0.00004
12	Bangombe	FRZ	BA.2-65.34 m	Sandstone	Galena inclusion in zircon	0.844	0.006	2.1750	0.0176	0.05362	0.00067
13	Bangombe	FRZ	BA.2-65.34 m	Sandstone	Galena inclusion in zircon	0.842	0.006	2.3030	0.0211	0.05294	0.00060
14	Bangombe	FRZ	BA.2-65.34 m	Sandstone	Galena inclusion in zircon	0.852	0.012	2.2180	0.0401	0.05463	0.00058
15	Bangombe	FRZ	BA.2-65.34 m	Sandstone	Zircon surrounding galena	0.798	0.005	2.3880	0.0138	0.04943	0.00051
16	Bangombe	FRZ	BA.2-570.57 m	Conglomerate	Galena	0.763	0.004	2.8440	0.0231	0.04627	0.00044
17	Bangombe	FRZ	BA.2-570.57 m	Conglomerate	Galena	0.765	0.005	2.9060	0.0499	0.04690	0.00093
18	Bangombe	FRZ	BA.2-570.57 m	Conglomerate	Galena intergrowth in pyrite	0.770	0.010	2.8340	0.0570	0.04900	0.00139

Table 7
Calculation of model age with $T_1 = 1.95$ Ga

Number	$^{207}Pb/^{206}Pb^{a}$	$\pm 2\sigma$	Age[a]	$\pm 2\sigma$	$^{235}U/^{238}U_{meas}$	$\pm 2\sigma$	Reference	$^{207}Pb/^{206}Pb^{a,b}$	$\pm 2\sigma$	Age[a,b]	
1	0.134	0.002	402	56	0.00710	0.00002	Gauthier-Lafaye et al., 1996	0.137	0.002	472	56
2	0.128	0.003	234	80	0.00710	0.00002	Gauthier-Lafaye et al., 1996	0.130	0.003	307	80
3	0.130	0.002	304	52	0.00710	0.00002	Gauthier-Lafaye et al., 1996	0.133	0.002	375	52
4	0.139	0.001	528	15	normal		Bros et al., 1995				
5	0.140	0.004	551	88	normal		Bros et al., 1995				
6	0.159	0.001	940	17	0.00678	0.00001	Holliger, 1991	0.170	0.001	1135	17
7	0.161	0.004	981	68	0.00678	0.00001	Holliger, 1991	0.172	0.004	1174	66
8	0.157	0.001	905	28	0.00678	0.00001	Holliger, 1991	0.168	0.002	1102	27
9	0.159	0.004	933	71	0.00678	0.00001	Holliger, 1991	0.170	0.004	1129	69
10	0.153	0.001	816	28	0.00678	0.00001	Holliger, 1991	0.163	0.002	1016	27
11	0.159	0.002	937	29	0.00678	0.00001	Holliger, 1991	0.170	0.002	1132	28

[a]Corrections have been made for common Pb ($^{206}Pb/^{204}Pb = 15.2$ at 1.95 Ga).
[b]Corrections have been made for ^{235}U depletion, from values found in the literature (see references).

Th being considered as an immobile element, the whole rock average Th/La ratio increase from 0.27 to 1.14 (Table 4) corresponds to the leaching of 76% of La during monazite dissolution. The average concentration of residual LREE of altered sandstones was 137 ppm (Table 4). Therefore, at the whole rock scale, an average of 434 ppm of LREE have been leached out. Consequently, at the Franceville basin scale, the global amount of LREE mobilized by diagenetic brines from FA coarse-grained sandstones represents approximately 2.01×10^9 metric tons. Since highly saline diagenetic fluids and detrital monazite are very common in deep sandstones basins, such an alteration should be widespread. Thus, if favorable traps do exist, large LREE deposits have to be expected in such environments.

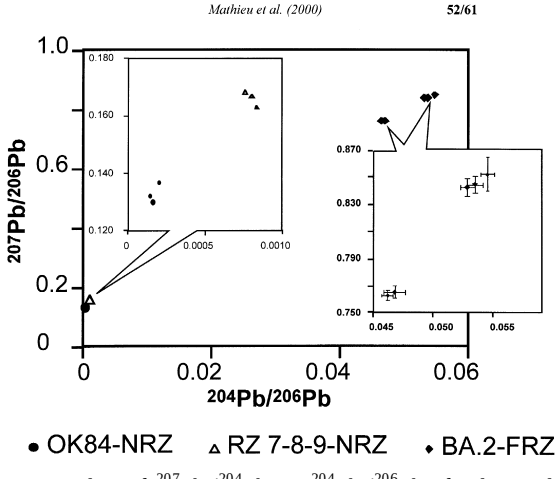

Fig. 12. Plots of $^{207}Pb/^{204}Pb$ vs. $^{204}Pb/^{206}Pb$ of galena only. OK84-NRZ (Near Rector Zone OK84) and RZ7-NRZ (Near Reactor Zone 7) have very radiogenic Pb, while BA.2-FRZ (Far from Reactor Zone, BA.2 borehole) has a composition comparable with average crust. The 2σ errors are, if not plotted, smaller or equal to the symbol size.

In order to estimate the amount of U specifically released from monazite, taking average U and LREE contents in non-altered monazite, respectively, 0.22% and 48.8% (Table 4), and 571 ppm (434 + 137) for the average concentration of LREE in FA sandstones before alteration, the average quantity of monazite in FA sandstones is therefore 1170 ppm ($571 \times 100/48.8$). Then, the U loss from monazite corresponds to 1.96 ppm ($76\% \times 1170 \times 0.22\%$). Finally, the amount of leached U only from monazite represents approximately 9.06×10^6 metric tons. This last result shows that the accessories dissolution process is largely sufficient to explain the total estimated U reserves (41,400 tons) of the Franceville basin (Gauthier-Lafaye, 1986). Furthermore, other U sources (possible detrital uraninites in the FA conglomerate, leaching of U-rich phases from the basement if we consider that the diagenetic brines have percolated below the sandstones basin) may also have been involved.

A more global estimation of the uranium can also be made using average Th/U ratio of sedimentary formations. Accordingly, using the increase of average Th/U ratios from 3.46 in unaltered metasedi-

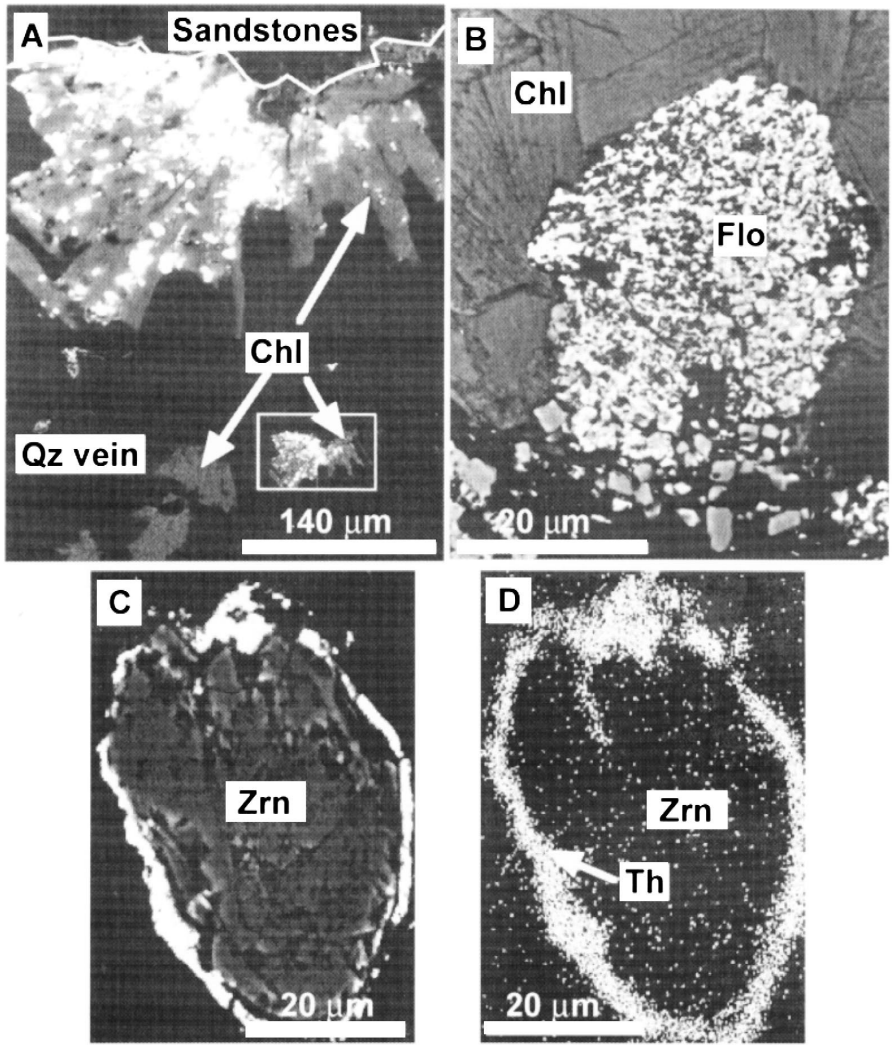

Fig. 13. BSE images of: (A) florencite microcrystals (Flo) located in diagenetic chlorite (Chl) of mineralized FA sandstones; (B) a (U,Zr)-silicate phase (white points) trapped in chlorite fibers (Chl) of a chlorite–quartz vein; and (C) a zircon crystal (Zrn) surrounding by a brighter zone corresponding to a Th-rich zone (Th) as seen in (D) with X-ray image of Th distribution.

ments to 14.2 in altered sandstones and an average residual concentration of uranium of 3 ppm (Table 4), the same calculations give 45.3×10^6 metric tons of leached uranium from the FA sandstones (Table 4). It corresponds not only to the leaching of U bound to monazite crystals, but also from uranium located in other sites because of the strong difference of Th/U ratio between fresh monazite (18.6; Table 4) and non-altered sandstones (3.03; Table 4). The estimation is also less reliable than the preceding one on LREE because the Th/U ratio from sedimentary rocks may be highly variable compared to the Th/La ratios.

6.4. Chronology of the events

6.4.1. Zircon crystallization and leaching of monazite and zircon

The U–Pb dating of zircon cores shows that detrital zircon in the FA formation has crystallisation

ages around 2.87 ± 0.05 Ga (Fig. 10). This is in good agreement with previous geochronological data obtained of the Archean basement in the area, e.g. 2.89 ± 0.04 Ga (Rb–Sr) ca. 75 km west of Oklo (Fig. 6; Caen-Vachette et al., 1988). Similar ages have been determined by U/Th/Pb chemical age on non-altered detrital monazite (2.51 ± 0.05 Ga; Fig. 6). They also agree with previous data, assuming that some Pb loss has occurred. The range of ages between 2.4 and 1.6 Ga may correspond to a re-equilibration during diagenesis and/or mineralization. Moreover, $^{207}Pb/^{206}Pb$ ratios of monazite from Oklo NRZ 7-8-9 sample (OBD.96-51) correspond to ages around 2.5 Ga (single-stage Pb growth; Ludwig, 1978). However, these Pb compositions must be used with caution, since the crystals have been severely altered, and there is evidence of massive Pb migrations in and around the reactor zones as shown in this paper and by Janeczek and Ewing (1995).

6.4.2. Pb mobility near the reactor zones

Pb mobility has occurred in and around the RZ after their formation (Janeczek and Ewing, 1995). The low $^{204}Pb/^{206}Pb$ ratios (Table 6) obtained on galena inclusions in zircon and monazite NRZ suggest that the source was rich in U relative to Pb. Considering an external origin of Pb (see discussion in Section 6.1), the most likely source is the surrounding 2 Ga U deposit. The samples are all located near RZ, which caused intense heat and hydrothermal circulations during criticality at 1.95 Ga. Therefore, in the two-stage model (Faure, 1986) used for age determinations of these galena crystals (T_2; see Table 7), T_1 has been set to 1.95 Ga. There are two complications with these age determinations: the proximity to the reactor zones, and the possible involvement of radiogenic Pb from monazite and zircon. The effects of the reactor zones, which are depleted in ^{235}U, can be estimated by correcting for the ^{235}U depletion reported in the literature. This correction is simply a multiplication of the $^{207}Pb/^{206}Pb$ with the ratio of normal $^{235}U/^{238}U$ to measured $^{235}U/^{235}U$. This correction yields older model ages, as seen in Table 7. Radiogenic Pb from detrital monazite and zircon should have a $^{207}Pb/^{206}Pb$ between ~ 0.37 (2 Ga) and ~ 0.25 (0.7 Ga). Assuming 3% (maximum; see Section 6.1) of the Pb comes from the in situ Pb of this composition, the corrected, slightly lower $^{207}Pb/^{206}Pb$ corresponds, on average, to model ages ca. 100 Ma younger than the ones reported in Table 7.

Therefore, the interpretation of these ages is that galena crystallized in zircon and monazite more than 1000 Ma later than the alteration event. The model ages spread from ca. 1000 Ma down to ca. 300 Ma, with an average around 680 Ma (Table 7). These ages are similar to the ages obtained previously by Holliger (1992), and indicate crystallization of galena and native lead, sometime after 1000 Ma. The two complications mentioned above, which might mix radiogenic Pb of different compositions, could be the reason for the scattered model ages. However, the scatter could also be due to the prolonged, regional heating in the basin in association with the intrusion of dolerite dykes between 1000 and 750 Ma. There is also a possibility that there is a second regional event indicated by the alteration of dolerite dykes (Weber and Bonhomme, 1975; Sère, 1996). If this is the case, uraninite might have suffered Pb loss twice, which would further complicate the U–Pb system.

6.4.3. Common Pb mobility deep in the basin

The common Pb composition deep in the Franceville basin, measured in galena inclusions in zircon, altered zircon (65 m depth), and epigenetic galena (570 m depth) indicates that the Pb source is not the uranium mineralization. The very unradiogenic composition in the altered zircon is evidence of its external origin; thus, Pb from external sources was emplaced in the zircon during or after its alteration. These external sources had Pb compositions similar to average crust.

One way for interpreting the data, called model A, is based on the petrographic and geochemical evidence that monazite and zircon were leached and dissolved during early diagenesis, which took place around 2 Ga. In model A, we assume that galena crystallized at 2 Ga with Pb from ca. 2.9 Ga old zircon and monazite. Thus, the radiogenic part of Pb should have a $^{207}Pb/^{206}Pb \approx 0.37$, which is equal to that produced in zircon, or any U-bearing system, from 2.9 to 2 Ga. The measured Pb does not have a radiogenic signature, and a large part of the Pb must therefore be common Pb. This common Pb, which was mixed with the radiogenic Pb at 2 Ga, has to have a very old signature in order to produce the

measured $^{207}Pb/^{206}Pb$ (0.76–0.84). If we correct for initial lead using the Stacey and Kramers Pb composition at 3.7 Ga ($^{207}Pb/^{204}Pb = 11.152$, $^{207}Pb/^{204}Pb = 12.998$), our measured samples will yield radiogenic $^{207}Pb/^{206}Pb$ in a range from 0.33 to 0.38, which is similar to what we would expect from the local zircon crystals at that time. Following model A, we see that common Pb in galena must come from two sources. The first would be a very old part of the basement (~ 3.7 Ga) which was leached of its initial lead (~ 3.7 Ga old Pb minerals) during the fluid circulations around 2 Ga. The second source would be radiogenic Pb produced in zircon and monazite, which were leached at ca. 2 Ga. There would have been no contribution from the 2.9 Ga old basement or host rock to the leached accessories during these events.

Thus, model A requires the interaction of a very old basement containing a ~ 3.7 Ga old Pb reservoir, which has never been described in the literature. The oldest age of Archean crust in Gabon reported in the literature is 3186 ± 75 Ma (Rb–Sr) (Caen-Vachette et al., 1988) from a gneiss in the North Gabon massif, some 300 km NW of Oklo. It also requires a process which would leach only isolated, initial Pb (= Pb minerals) from this old basement. There is also a need to explain how galena can crystallize during conditions that leach U from zircon and monazite.

Therefore, we have to consider another model, called model B, in which we assume that galena crystallization occurred sometime later than 2 Ga. The arguments against this model are that the Franceville basin was highly silicified after the diagenesis and mineralization, which reduced the porosity of the sandstone. Also, description of any event of element mobility later than 2 Ga, in the deep parts of the FA formation, is lacking in the literature.

However, Pb mobility has occurred in the uranium deposits and reactor zones later than 1000 Ma (Janeczek and Ewing, 1995; Gauthier-Lafaye et al., 1996), due to the intrusion of a dolerite dyke swarm at 1000–750 Ma. Thus, we see that there is at least one possible time for galena crystallization after 1000 Ma. There was also a later chloritization of these dykes, proposed to have occurred around 500 Ma by Weber and Bonhomme (1975), but the effect of this alteration event overall the Francevillian basin is not known. The question is if our Pb isotope data are compatible with galena crystallization after 1000 Ma. The regressed line through the galena samples on a normal $^{207}Pb/^{204}Pb$ vs. $^{206}Pb/^{204}Pb$ diagram has a slope of ca. 0.23, and cuts the Stacey and Kramers (1975) growth curve at ~ 2880 and ~ 540 Ma. Unfortunately, the error on this "isochron" is too large for any reasonable age determination. Assuming that initial Pb is Pb that was put into the basement when it formed, we can calculate galena model ages. Correcting for initial Pb with composition $^{207}Pb/^{204}Pb = 14.469$ and $^{206}Pb/^{204}Pb = 13.169$ (Stacey and Kramers, 1975 Pb at $T_1 = 2.9$ Ga), these ages range from 803 to 253 Ma, with very large errors. Two galena model ages with 2σ errors less than 50% yield ages of 803 ± 392 Ma (no. 13; Table 6), and 591 ± 195 Ma (no. 16; Table 6).

Even if the "isochron" and the model ages have very large errors, they indicate a time of galena crystallization later than 1000 Ma, if the Pb was withdrawn from a U–Pb system that formed at ~ 2.9 Ga. Thus, model B can explain the observed Pb compositions, and it involves known geological events and formations: the basement and the dolerite dykes. Following model B, galena in zircon and monazite was crystallized during the same period both in the uranium ores and far from them. Model B involves a simplified U–Pb system and eliminates the need (in model A) for an unknown, ~ 3.7 Ga old, Pb reservoir. Also, it eliminates the need to explain the simultaneous leaching of U and crystallization of galena in the accessories.

Considering the advantages and weaknesses of models A and B, we conclude that galena crystallization was a secondary process occurring in already altered accessories, as well as in the host rock. Sometime after 1000 Ma, around the time of the dolerite dyke intrusions, galena crystallized both in the U ores and deeper down in the Franceville basin.

7. Conclusions

Most of previous works on Oklo have been focused on the near field of reactor zones. These studies have evidenced migration and incorporation of fissiogenic Zr, REE, Nd, Cs, Sm, Sr and Pu, U, Th in several accessory minerals. The present work

has extended these studies to the far field to evaluate the magnitude of the migration of some elements (REE, Th, U, Zr and Pb) which represent natural analogs of the radiotoxic nuclides. It is shown that accessory minerals present different retention capacities for the actinides and lanthanides. Monazite is extensively dissolved and zircon is altered to a lesser extend.

During early diagenesis, the alteration concerns accessory-rich layers in the coarse-grained FA sandstones all over the Franceville basin. At that time, the circulation of highly saline and oxidizing brines is responsible for monazite dissolution and leaching of LREE, U and P and the strong increase of the Th/U ratios from monazite to newly formed Th–OH-silicate. The high chloride concentration of the brines suggests a complexation of REE and uranium by chlorides. But, the simultaneous dissolution of LREE, U and P during monazite alteration and the crystallization of fluorapatite and florencite in other parts of the basin indicate that phosphate and fluoride complexes may have also played an important role in the transportation of uranium and rare earths in basinal brines.

REE and U leaching is also attested by the variation of Th/La and Th/U ratios at whole rock scale comparing altered rocks with unaltered equivalents in the basin and from the literature. Early diagenesis has affected at least the coarse-grained layers, because probably of their higher permeability during diagenesis. Calculated maximum LREE and U release from monazite–whole rock balance at 2.01×10^9 and 9.06×10^6 metric tons, respectively.

Zircon crystals are mainly altered at their rims which were enriched in P and Th, U, REE, respectively, replacing Si and Zr–Hf. U–Pb dating of unaltered cores of detrital zircon crystals gives ages around 2.87 ± 0.05 Ga, in agreement with Archean basement ages from which the Francevillian sediments are derived.

In the altered areas of monazite and zircon, galena occurs as tiny inclusions or in crack fillings. The global amount of lead contained as galena in the accessory minerals largely exceeds the amount of lead produced in situ by radioactive decay of U and Th in these minerals and thus, has an external origin. The altered part of zircon and galena inclusions in zircon at 65 m depth in the BA.2 borehole, and epigenetic galena crystals dispersed in the sandstone at 570 m depth have all Pb isotopic compositions comparable to average crust which confirm an external origin of Pb. Pb isotopic compositions of galena indicate a crystallization age sometime after 1000 Ma, both in the U ores and far from them. Thus, galena crystallized in the already altered parts of monazite and zircon during an event, clearly distinct, from the 2 Ga event corresponding to accessory mineral alteration during early diagenesis. Galena crystallization probably occurred during the regional extension and intrusion of a dolerite dyke swarm, which intruded between 1000 and 750 Ma.

Acknowledgements

Part of this research was conducted while the first author was a doctoral research fellow at the Research Center on the Geology of Mineral and Energetical Resources (CREGU) and Henri Poincaré-Nancy I University. Completion of this work was funded by a contract between CEA and CREGU in the frame of the “Oklo, Natural Analogue Phase II” project within the 4th Program of Coordinated Research and Development of the European Commission. The second author was funded by the Swedish Nuclear Fuel and Waste Management (SKB) .

We also thank A. Kohler, R. Podor and S. Barda (University of Nancy I) for technical assistance with SEM and electron microprobe determination. We thank the staff of the NORDSIM facility: S. Claesson, T. Sunde, M. Whitehouse and J. Vestin, for technical assistance and helpful discussions. This is NORDSIM contribution no. 23.

L.A. Neymark and M. Pagel are thanked for helpful reviews of this manuscript.

References

Akers, W.T., Grove, M., Harrison, T.M., Ryerson, F.J., 1993. The instability of rhabdophane and its unimportance in monazite paragenesis. Chem. Geol. 110, 169–176.

Alderthon, D.H.M., Pearce, J.A., Potts, P.J., 1980. Rare earth element mobility during granite alteration: evidence from Southwest England. Earth Planet. Sci. Lett. 49, 149–165.

Belshaw, N.S., O’Nions, R.K., Martel, D.J., Burton, K.W., 1994.

High-resolution SIMS analysis of common lead. Chem. Geol. 112, 54–70.

Bonhomme, M., Leclerc, J., Weber, F., 1978. Etude radiochronologique complémentaire de la série du Francevillien et de son environnement. Les Réacteurs de Fission Naturels. IAEA, Vienne, pp. 19–23, TC-119/9.

Bonhomme, M., Gauthier-Lafaye, F., Weber, F., 1982. An example of Lower Proterozoic sediments. Precambrian Res. 18, 87–102.

Bros, R., Stille, P., Gauthier-Lafaye, F., Weber, F., Clauer, N., 1992. Sm–Nd isotopic dating of Proterozoic clay material: an example from the Francevillian sedimentary series, Gabon. Earth Planet. Sci. Lett. 113, 207–218.

Bros, R., Turpin, L., Gauthier-Lafaye, F., Holliger, Ph., Stille, P., 1993. Occurrence of naturally enriched 235 uranium: implications for Pu behaviour in natural environments. Geochim. Cosmochim. Acta 57, 1351–1356.

Bros, R., Gauthier-Lafaye, F., Larque, P., Samuel, J., Stille, P., 1995. Mobility of uranium, thorium and lanthanides around the Bangombé natural nuclear reactor zone (Gabon). Mater. Res. Soc. Symp. Proc. 353, 1187–1194.

Caen-Vachette, M., Vialette, Y., Bassot, J.P., Vidal, P., 1988. Apport de la géochronologie isotopique à la connaissance de la géologie gabonaise. Chron. Rech. Min. 491, 35–54.

Cathelineau, M., Boiron, M.C., Holliger, Ph., Poty, B., 1990. Metallogenesis of the French part of the variscan orogen. Part II: Time–space relationships between U, au and Sn–W ore deposition and geodynamic events, mineralogical and U–Pb data. Tectonophysics 177, 59–79.

Compston, W., Williams, I.S., Meyer, C.E., 1984. U–Pb geochronology of zircons from lunar breccia 73217 using a sensitive high-mass resolution ion microprobe. Geophys. Res. B 89, 525–534.

Daly, R.A., Manger, G.E., Clark, S.P., 1966. In: Clark, S.P (Ed.), Handbook of Physical Constants. pp. 20–26.

Dimroth, E., 1979. Significance of diagenesis for the origin of Witwatersrand-type uraniferous conglomerates. Proc. R. Soc. London, Philos. Trans., Ser. A 291, 277–287.

Dymkov, Y., Holliger, Ph., Pagel, M., Gorshkov, A., Artyukhina, A., 1997. Characterization of a La–Ce–Sr–Ca aluminous hydroxy phosphate in nuclear zone 13 in the Oklo uranium deposit (Gabon). Miner. Deposita 32, 617–620.

Faure, G., 1986. Principles of Isotope Geology. Wiley and Sons, New York, p. 589.

Fayek, M., Kyser, T.K., 1997. Characterization of multiple fluid flow events and rare earth element mobility associated with formation of unconformity-type uranium deposits in the Athabasca basin, Saskatchewan. Can. Mineral. 35, 627–658.

Fedo, C.M., Eriksson, K.A., Krogstad, E.J., 1996. Geochemistry of shales from the Archean (3 Ga) Buhwa greenstone belt, Zimbabwe: implications for provenance and source-area weathering. Geochim. Cosmochim. Acta 60, 1751–1763.

Gancarz, A.J., 1978. U–Pb age (2.05×10^9 years) of the Oklo uranium deposit. Les Réacteurs de Fission Naturels. IAEA, Vienne, pp. 513–520, TC-119/40.

Gauthier-Lafaye, F., 1986. Les gisements d'uranium du Gabon et les réacteurs d'Oklo. Modèle métallogénique de gîtes à fortes teneurs du Protérozoique inférieur. Mem. Sci. Geol. 78, 206.

Gauthier-Lafaye, F., Weber, F., 1989. The Francevillian (Lower Proterozoic) uranium ore deposit of Gabon. Econ. Geol. 84, 2267–2268.

Gauthier-Lafaye, F., Holliger, Ph., Blanc, P.L., 1996. Natural fission reactors in the Franceville basin, Gabon: a review of the conditions and results of a "critical event" in a geologic system. Geochim. Cosmochim. Acta 60, 4831–4852.

Gerard, B., Royer, J.J., Le Carlier de Veslud, C., Pagel, M., 1998. Modélisation 3D des transferts thermiques et fluides autour d'un réacteur naturel de fission (Oklo, Gabon). Bull. Soc. Geol. France 169, 459–466.

Gibbs, A.K., Montgomery, C.W., O'Day, P.A., Erslev, E.A., 1986. The Archean–Proterozoic transition: evidence from the geochemistry of metasedimentary rocks of Guyana and Montana. Geochim. Cosmochim. Acta 50, 2125–2141.

Govindaraju, K., Mevelle, G., 1987. Fully automated dissolution and separation methods for inductively coupled plasma emission spectrometry rock analysis. Application to the Determination of Rare Earth Elements. J. Anal. Atom. Spectrosc. 2 pp. 615–621.

Harrison, T.M., Mc Keegan, K.D., Lefort, P., 1995. Detection of inherited monazite in the Manaslu leucogranite by $^{208}Pb/^{232}Th$ ion microprobe dating: crystallization age. Earth Planet. Sci. Lett. 133, 271–282.

Holliger, Ph., 1988. Ages U/Pb définis in situ sur oxydes d'uranium à l'analyseur ionique: méthodologie et conséquences géochimiques. C. R. Acad. Sci. Paris 307 (2), 367–373.

Holliger, Ph., 1991. Systématique U/Pb et étude isotopique in situ ^{235}U-produits de fission de la zone de réaction hybride SF29 (zone 10). Autres zones d'intérêt sur le site d'Oklo pour les études futures. Note technnique DEM N°10/91, CEREM, Grenoble, 35 pp.

Holliger, Ph., 1992. Geochemical and isotopic characterization of the reaction zones (uranium, transuranium, lead and fission products). Proc. 2nd Joint CEC–CEA Meet., Brussels, Belgium, 27–38.

Janeczek, J., Ewing, R.C., 1995. Mechanisms of release from uraninite in the natural fission reactors in Gabon. Geochim. Cosmochim. Acta 59, 1917–1931.

Janeczek, J., Ewing, R.C., 1996a. Phosphatian coffinite with rare earth elements and françoisite-(Ce,Nd) from sandstones beneath a natural fission reactor at Bangombé (Gabon). Mineral. Mag. 60, 665–669.

Janeczek, J., Ewing, R.C., 1996b. Florencite-La with fissiogenic REEs from a natural fission reactor at Bangombé (Gabon). Am. Mineral. 81, 1263–1276.

Jefferies, N.L., 1985. The distribution of rare earth elements within Carnmenellis Pluton, Cornwall. Mineral. Mag. 49, 495–504.

Kingsbury, J.A., Miller, C.F., Wooden, J.L., Harrison, T.M., 1993. Monazite paragenesis and U–Pb systematics in rocks of the eastern Mojave Desert, California, USA: implications for thermochronometry. Chem. Geol. 110, 147–167.

Krauskopf, K.B., 1986. Thorium and rare earth metals as analogs for actinide elements. Chem. Geol. 55, 323–335.

Ludwig, K.R., 1978. Uranium daughter migration and U/Pb isotope apparent ages of uranium ores Shirley basin, Wyoming. Econ. Geol. 73, 29–49.

Mc Lennan, S.M., Taylor, S.R., 1979. Rare earth element mobility associated with uranium mineralization. Nature 282, 247–250.

Mc Lennan, S.M., Hemming, S.R., Taylor, S.R., Eriksson, K.A., 1995. Early Proterozoïc crustal evolution: geochemical and Nd–Pb isotopic evidence from metasedimentary rocks, southwestern North America. Geochim. Cosmochim. Acta 59, 1153–1177.

Mathieu, R., Cathelineau, M., Cuney, M., Gauthier-Lafaye, F., Pourcelot, L., Pironon, J., Fabre, C., Vallance, J., 2000. Geochemistry of fluid paleocirculations in the Franceville basin associated to diagenesis and uranium mineralization (Oklo, Gabon). Econ. Geol., Submitted.

Montel, J.M., Foret, S., Veschambre, M., Nicollet, C., Provost, A., 1996. Electron microprobe dating of monazite. Chem. Geol. 131, 37–53.

Naudet, R., 1991. Des Réacteurs Nucléaires Fossiles. In: Eyrolles (Ed.). Paris (coll. CEA), 1991, 695 pp.

Openshaw, R., Pagel, M., Poty, B., 1978. Phases fluides contemporaines de la diagenèse des grès, des mouvements tectoniques et du fonctionnement des réacteurs nucléaires d'Oklo (Gabon). Les Réacteurs de Fission Naturels. IAEA, Vienne, pp. 267–296, TC-119/9.

Peycelon, H., 1995. Oklo, analogue naturel. Reconstitution des circulations fluides anciennes par la géochimie des éléments en traces: du champ proche au champ lointain. Thesis, Ecole des Mines de Paris, 175 pp.

Pouchou, J.L., Pichoir, F., 1984. Un nouveau modèle de calcul pour la microanalyse quantitative par spectrométrie de rayons X. La Recherche Spatiale 3, 167–192.

Raimbault, L., 1998. Remplissages fissuraux à Okélobondo, données analytiques et interprétations préliminaires. Rapport d'avancement LHM/RD/98/27, 1998, 79 pp.

Raimbault, L., Peycelon, H., Blanc, P.L., 1996. Characterization of near-to far-field ancient migrations around Oklo reaction zones (Gabon), using minerals as geochemical tracers. Radiochim. Acta 74, 283–287.

Ribeiro, M.D.A., 1999. Estudo litogeoquimico das formaçoes metasedimentares encaixantes de mineralizaçoes em Tras-os-Montes Ocidental, implicaçoes metalogénicas. Thesis, Universidade do Porto, 231 pp.

Robinson, A., Spooner, E.T.C., 1984. Postdepositional modification of uraninite-bearing quartz–pebble conglomerates from the Quirke ore zone, Elliot Lake, Ontario. Econ. Geol. 79, 297–321.

Roscoe, D., 1969. Huronian rocks and uraniferous conglomerates in the Canadian Shield. Can. Geol. Survey 68-40, 205 pp.

Rubin, J.N., Henry, C.D., Price, J.G., 1993. The mobility of zirconium and other "immobile" elements during hydrothermal alteration. Chem. Geol. 110, 29–47.

Ruffenach, J.C., 1979. Les réacteurs naturels d'Oklo: paramètres neutroniques, date et durée de fonctionnement, migration de l'uranium et des produits de fission. Thesis, Univ. Paris VII, 350 pp.

Savary, V., Pagel, M., 1997. Redox conditions in the natural fission reactor zones from Oklo (Gabon): the influence of radiolysis. Geochim. Cosmochim. Acta 61, 4479–4494.

Schidlowski, M., 1981. Uraniferous constituents of the Witwatersrand conglomerates: ore-microscopic observations and implications for the Witwatersrand metallogeny. U.S. Geol. Survey, 29 pp., 1161-N.

Sère, V., 1996. Géochimie des minéraux néoformés à Oklo (Gabon): histoire géologique du bassin d'Oklo, une contribution pour les études de stockages géologiques de déchets radioactifs. Thesis, Univ. Paris VII, 278 pp.

Smith, H.A., Barreiro, B., 1990. Monazite: U–Pb dating of staurolite grade metamorphism in pelitic schists. Contrib. Mineral. Petrol. 105, 602–615.

Stacey, J.S., Kramers, J.D., 1975. Approximation of terrestrial lead isotope evolution by a two-stage model. Earth. Planet. Sci. Lett. 26, 207–221.

Walton, R.D., Cowan, G.A., 1975. Relevance of nuclide migration at Oklo to the problem of geologic storage of radioactive waste. Le Phénomène Oklo. IAEA, Vienne, pp. 499–507, SM-204/1.

Weber, F., Bonhomme, G.A., 1975. Donnnées radiochronologiques nouvelles sur le Francevillien et son environnement. Le Phénomène Oklo. IAEA, Vienne, p. 647, SM-204/1.

Weber, F., 1969. Une série précambrienne du Gabon: le Francevillien, sédimentologie, géochimie, relations avec les gîtes minéraux. Mem. Sci. Geol. 28, 328.

Wood, S.A., Williams-Jones, A.E., 1994. The aqueous geochemistry of the rare earth elements and yttrium. Monazite solubility and REE mobility in exhalative massive sulfide-depositing environments. Chem. Geol. 115, 47–60.